CHAPTER 4

APPLICATION OF PURE ZnO AND Nb-DOPED ZnO
FOR USE AS GAS SENSORS

Gases are the key measure in many industrial and domestic activities. In the last decade the specific demand for gas detection and monitoring has emerged particularly as the awareness of the need to protect the environment has grown. Gas sensors find applications in numerous fields [1−2]. Two important groups of applications are the detection of single gases (as NO_x, NH_3, O_3, CO, CH_4, H_2, SO_2, etc.) and the discrimination of odors or generally the monitoring of changes in the ambient. Single gas sensors can, for examples, be used as fire detectors, leakage detectors, controllers of ventilation in cars and planes, alarm devices warning the overcoming of threshold concentration values of hazardous gases in the work places.

Resistive-type gas sensors based on thin films of metal oxides have been intensively investigated in the last few years. The sensor performance can be improved by the incorporation of different additives to the films. They can participate directly in the gas–solid interaction by means of a chemical or electronic mechanism [3], thus favoring the adsorption of gas molecules on the surface. As a consequence, the gas surfaces coverage increases and the electrical conductivity changes. In addition, a decrease of the working temperature for the highest sensitivity is generally observed.

Existing gas sensors have been fabricated using a variety of metal oxide semiconductors (e.g., SnO_2, ZnO, WO_3, In_2O_3, V_2O_5, TiO_2, etc.) as gas-sensing materials [4–9]. Metal-oxide semiconductors have low operating temperatures, high response and easy to operate; therefore, these semiconductors can approximately be divided in determine their suitability for use as gas sensors [10–12].

Nitrogen dioxide (NO_2) gas is a common air pollutant important for monitoring environmental pollution produced during combustion in automotive engines, industrial factories, and power plants [13]. Health and safety guidelines suggest that when the concentration of NO_2 is higher than 3 ppm, it is dangerous to the human body and is thought to cause asthma at significantly lower levels; the effects of an exposure to NO_2 include factory paralysis and deterioration in health [14–16]. In recent years, the concentration of NO_2 in atmosphere has increased. NO_2 causes lung irritations, decreases the fixation of oxygen molecules on red blood cells, increases the susceptibility to infections, contributes to acid rains and plays an important role in the formation of ozone in the lower atmosphere [17]. Therefore, the development of a reliable sensor that can effectively detect even with extremely low concentration of NO_2 with high response is highly desirable. Such a sensor can be used for environmental monitoring. These advantages to the development of sensors can detect extremely low concentrations of NO_2.

To the best of our knowledge, the application of Nb-doped ZnO nanoparticles as gas sensor has not been reported yet. In this study, the gas-sensing capability of undoped ZnO and Nb-doped ZnO nanoparticles as gas sensor was demonstrated for NO_2, CO, C_2H_5OH and acetone and the responsible gas-sensing mechanism was suggested.

4.1   Introduction

Most widely studied area of solid-state gas sensors is that based on semiconducting oxides. A semiconductor gas sensor usually utilizes a porous sintered block body consisting of polycrystalline particles of a semiconducting oxide such as SnO_2, WO_3, ZnO, and In_2O_3: Recently, thick- and thin-film-type sensors have also been investigated for miniaturizing sensor elements by micro-fabrications. In Figure 4.1 examples of block- or film-type devices and the polycrystalline particles involved in the devices are illustrated [18].
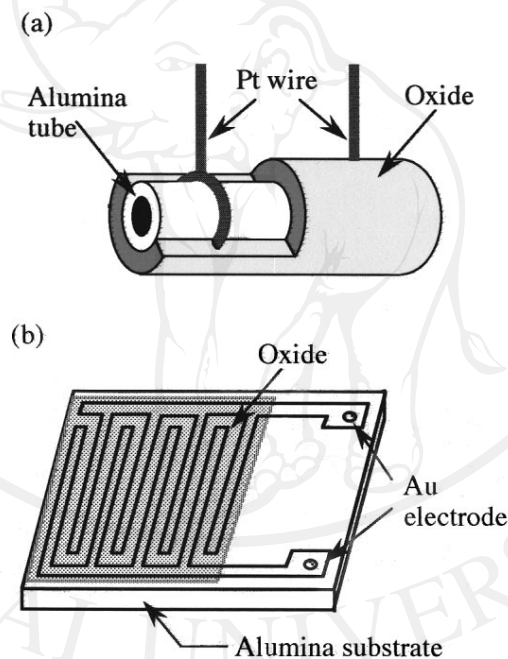

Figure 4.1 Schemetic drawings of sensor devices (a) sintered block type, (b) thick- or thin-film type [18].

Usually the devices for laboratory tests are furnished with a heater so that they are heated externally to obtain an optimum operating temperature. Upon exposure to a particular gas (target gas) of a low concentration in air, the sensor changes its electrical resistance. The resistance change is caused by a loss or a gain of surface electrons as a result of adsorbed oxygen reacting with the target gas. If the oxide is an

n-type, there is either a donation (reducing gas) or subtraction (oxidising gas) of electrons from the conduction band. The result is that n-type oxides increase their resistance when oxidising gases such as NO_2, O_3 are present while reducing gases such as CO, CH_4, C_2H_5OH, acetone lead to a reduction in resistance. The converse is true for p-type oxides, such as Cr_2TiO_3.
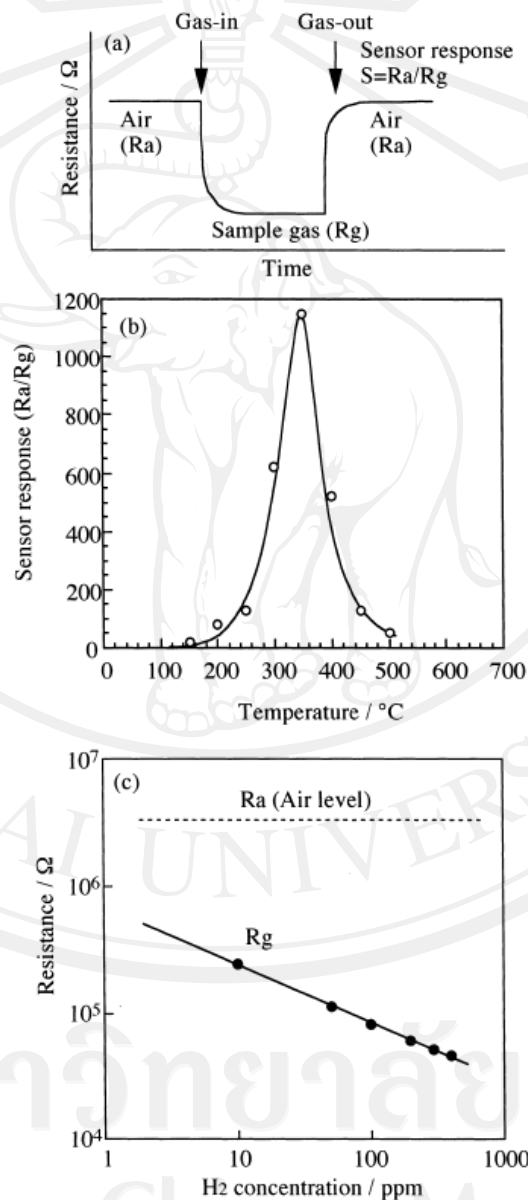

Figure 4.2 Typical characteristics of semiconductor gas sensor: (a) response transient; (b) temperature dependence of gas response; (c) dependence of Rg on gas concentration [18].

When this experiment is carried out in a flow apparatus, reducing gases can obtain response transients like those shown in Figure 4.2(a). The change in the electrical resistance is from a level in air (R_a) to a steady level (R_g) on exposure to the target gas and vice versa on cutting off the gas flow. There are two important characteristics of the gas sensor in these transients, i.e., the gas response (S) (often called sensitivity) defined as:

$$S = \frac{R_a}{R_g} \tag{4.1}$$

and the rates of response and recovery. The gas response (R_a/R_g) is very much dependent on the operating temperature, going through a maximum for an inflammable gas as shown in Figure 4.2(b). Naturally R_g as well as R_a/R_g depend on the kind and concentration of target gas besides other conditions. As illustrated in Figure 4.2(c), R_g and gas concentration are usually correlated linearly in a log–log scale. For oxidizing gases, the response (S) is defined as:

$$S = \frac{R_g}{R_a} \tag{4.2}$$

Equation 4.3 shows the response dependence of concentration of gas.

$$S = aC^m \tag{4.3}$$

where a is the variation constant.

The conductivity is enhanced by the adsorption of electron accepting gas molecules. The temperature dependence of the conductivity is formally expressed by

$$\sigma = \sigma_o \exp\left(-\frac{qV_S}{k_B T}\right) \tag{4.4}$$

where σ is the conductivity, σ_o is a constant independent of temperature, V_s is potential barrier, q is electric charge, k is the Boltzmann constant and T is the absolute temperature.

Semiconductor gas sensors have been investigated extensively for the purpose of practical applications, such as gas leak detectors and environmental monitoring. Since the pioneering works reported in 1962 by Seiyama et al. [19] and Taguchi [20], much technological effort has been made in this field, aiming at improvement in gas response, selectivity, stability, and feasibility for practical use. Yet further innovations of gas sensing properties are still in great demand to expand the fields of gas sensor applications. Numerous kinds of gases are emitted from various sources into our living space, working space, or outdoors. Many of them are hazardous to human beings and the environment, like air pollutants, while some others can be used as measures to diagnose the state of their sources, like ethanol and acetone in the breath and flavor components of foods. Most of these gases are present at very low concentrations so that extremely good sensing characteristics are required for their monitoring. In order to realize such gas sensors, it seems imperative to establish the principles of sensor design on the basis of fundamental understandings of semiconductor gas sensors. It is the aim of the present article to describe the state of the art of sensor design in the hope of further advancement of semiconductor gas sensors.

4.1.1 Gas sensing mechanism

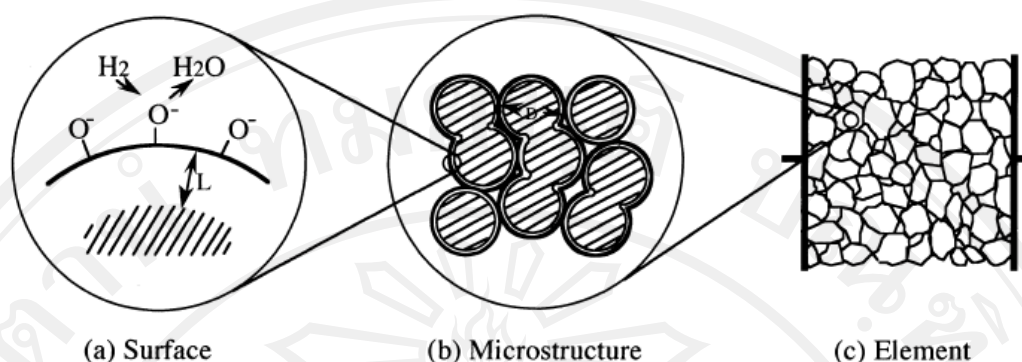The process of gas sensing by a semiconductor device illustrated in Figure 4.3.

Figure 4.3 The adsorbed molecule can significantly modify the dielectric property at the surface of the semiconductor gas sensor [18].

Owing to the large surface-to-volume ratio of the metal oxide nanoparticles such as ZnO nanoparticles (which will be used as the model for the mechanism of gas sensors), the conductance is very sensitive to the change in surface chemistry. As a molecule being adsorbed on nanoparticles surfaces, charge transfer can occur between the adsorbate and the adsorbent. The adsorbed molecule can significantly modify the dielectric property at the surface, which greatly affects the surface conductance. Therefore, nanoparticles materials can result in a huge improvement in gas sensing performances. In case of n-type metal oxide sensor, this interaction is commonly attributed to a redox reaction between the target gas and adsorbed oxygen [21]. As we all know, the sensor response is determined mainly by the quantity of active sites on the surface of gas sensors. When a ZnO nanoparticles sensor is exposed to air, oxygen molecules adsorb on the surface of the materials to form O_2^-, O^-, O^{2-} ions by capturing electrons from the conductance band, Thus the ZnO nanoparticles sensors show a high resistance in air.

$$O_2(gas) \quad \rightarrow \quad O_2(ads) \tag{4.5}$$

$$O_2(ads) + e^- \quad \rightarrow \quad O_2^-(ads) \tag{4.6}$$

$$O_2^-(ads) + e^- \quad \rightarrow \quad 2O^-(ads) \tag{4.7}$$

$$O^-(ads) + e^- \quad \rightarrow \quad O^{2-}(ads) \tag{4.8}$$

When the ZnO nanoparticles sensor is exposed to a reductive gas (such as CO) at moderate temperature, the target gas reacts with the surface oxygen species. The reaction can result in a decrease in the amount of surface O_2^-, O^-, and O^{2-} ions, the reaction can be described as follows:

$$R + O^-(ads) \quad \rightarrow \quad RO + e^- \tag{4.9}$$

Thus leads to an increase in concentration of electrons. This eventually increases the conductivity of the ZnO nanoparticles. When the material exposed to the atmosphere of NO_2, NO_2 can not only capture the electronics of the semiconductor due to its higher electrophilic property, but also react with the adsorbed oxygen ion leading to the formation of adsorbed NO_2^-, the process of the reaction can be described as follows:

$$NO_2(g) + e^- \rightarrow NO_2^-(ads) \tag{4.10}$$

$$NO_2(g) + O_2^-(ads) + 2e^- \rightarrow 2NO_2^-(ads) + 2O^-(ads) \tag{4.11}$$

The above reactions were all decreased the concentration of electron on the surface of the material, thus results in an increase of the material resistance. In addition, the reaction is happened between $NO_2^-(ads)$ and $O_2^-(ads)$:

$$NO_2^-(ads) + O_2^-(ads) \rightarrow 2O_2^-(ads) + NO_2 \tag{4.12}$$

Thus the cycling reaction continues:

$$NO_2(g) + e^- \rightarrow NO_2^-(ads) \tag{4.13}$$

These series of reactions resulted in the concentration of electron on the surface of the material further decreases, which led to the conductivity decrease of the material (increase of the resistance), then the detection of NO_2 is achieved.

Figure 4.4(a) shows a schematic diagram of a channel composed of the as-pasted ZnO nanoparticles with a relatively thin electron depleted layer under dry air ambient. When the NO_2 gas molecules are adsorbed on the surfaces of the ZnO nanoparticles, some of the electrons within them are transferred to the gas molecules and the electron depleted layer is broadened in the channel, resulting in higher and wider junction potential barriers. This mechanism is illustrated in Figure 4.4(b). Under the dry air ambient, the resistance measured for the channel composed of the heat-treated ZnO nanoparticles. After the as-pasted nanoparticles were heat-treated at 400ºC, the nanoparticles became larger and necked. Consequently, the number of junctions decreased, because of the increase in the size of the nanoparticles, and the height of the junction potentials was reduced, due to their physical necking, as illustrated in Figure 4.4(c). Figure 4.4(d) shows a schematic diagram of the heat-treated nanoparticles and the junction potential under the target NO_2 gas ambient. The junction potential barriers present at the necked parts of the nanoparticles are still too high and too wide for the electrons to jump over the barrier, so that the reduction in the number of junctions may not contribute significantly to the decrease in the resistivity under the target gas ambient [22].
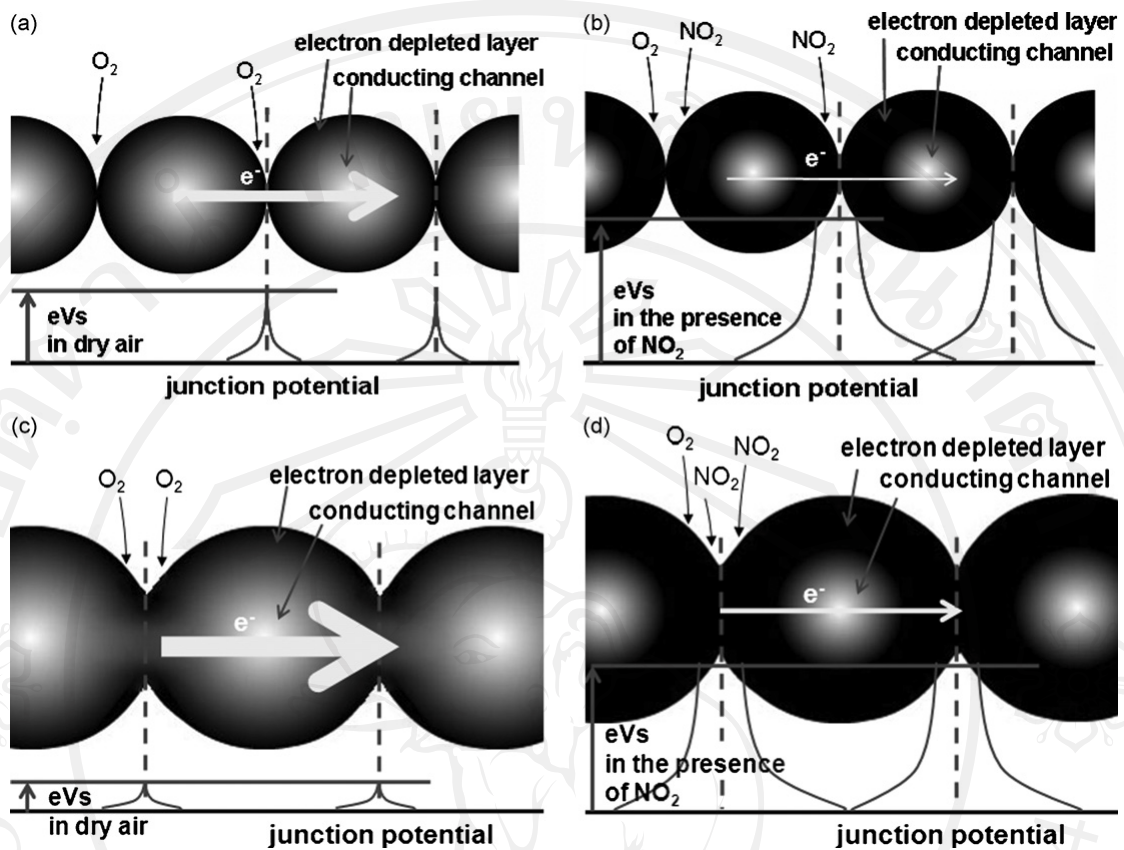
Figure 4.4 Schematic diagrams of the as-pasted ZnO nanoparticles (a) under dry air ambient and (b) under NO_2 gas mixed dry air ambient, and of the heat-treated ZnO nanoparticles (c) under dry air ambient and (d) under NO_2 gas mixed dry air ambient. The schematic junction potentials are drawn in the diagrams. The arrow at the center of each of the figures represents the current flow at a certain applied voltage, and the thickness of the arrow represents the relative magnitude of the measured current flow [22].

4.1.2 Temperature Limitations [23]

All sensors and electronics have ambient temperature limitations. The installation of the sensor must be within the operating range of each. If the area is too hot for the electronics, a sensor extension kit is available to separate the sensor from

the transmitter/remote calibration modules. If the gas temperature is too hot for the sensor, a gas reclamation adapter is available to draw air samples to the sensor. By connecting metal coils to the inlet side of this adapter, the gas can be cooled down. If any preconditioning system is to be used, make sure that the vapors will not condense in the piping.

4.1.3 Response and recovery time [23]

Although sensor output is linear, response time is a logarithmic function. The first molecules of gas to diffuse through the membrane cause a very rapid change in response; as the sensor's output approaches the actual ambient gas concentration, the rate of change of response slowly decreases. The response curve of the best sensors looks very much like a step function; that it looks more like a straight line. The inverse of the response curve determines a sensor's recovery time after being exposed to gas.
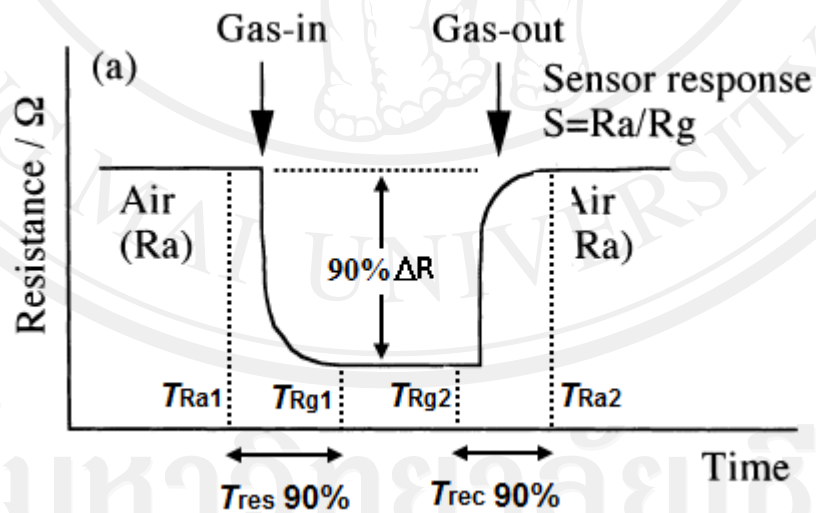

Figure 4.5 The response and recovery time of n-type semiconductor for reducing gas [18].

Manufacturers typically define some length of time, such as 10 minutes, as the point at which a sensor reaches its maximum output. A sensor's T_{90} is the times to reach 90% variation in resistance upon exposure to gas and air were defined as the 90% response time ($T_{90\%}$(air-to-gas)) and 90% recovery time ($T_{90\%}$(gas-to-air)), respectively,

The response and recovery time of n-type semiconductor for reducing gas can be calculated (Equations 4.14 and 4.15) as follows:

$$T_{res} = [T_{Ra1} - \{(T_{Ra1} - T_{Rg1})\} \times \frac{90}{100}] - T_{Ra1} \qquad (4.14)$$

$$T_{rec} = [T_{Rg2} + \{(T_{Ra2} - T_{Rg2})\} \times \frac{90}{100}] - T_{Rg2} \qquad (4.15)$$

4.1.4 Selectivity [23]

Selectivity is the ability of a sensor to measure only one parameter, in the case of a chemical sensor, to measure only one chemical species. The sensitivity of certain gas sensors to different gases depends on the choice of catalytic sensor material and the operating temperature. By combining several different gas sensors into a sensor array, complex gas mixtures can be analyzed

4.1.5 Metal additives affect

Recently, there are also many reports on the enhancement of gas response by catalyzing or doping of metal-oxide semiconductor nanoparticles with noble metal nanoparticles such as Pd, Ru, or Au [24–25]. Moreover, the additives can increase the material porosity, thus increasing the specific surface area suitable for gas adsorption and, consequently, the sensor response. Despite the mentioned positive effect, the use of additives might provoke an increase in the electrical resistance of the metal oxide films. In fact, NO_2 is an oxidizing gas and it induces a resistance increase on an n-type

semiconductor. The increase of sensor impedance is a non-desired effect, since a complicated associated electronic circuitry is required when it exceeds about 10 MΩ. Therefore, the sensitization of sensors by using additives which decrease the electrical resistivity of films via a doping mechanism may be a good solution. However, the increase of the carrier concentration associated to doping would decrease the fractional change of the resistance in the target gas and air, which would also decrease the sensor response [26].

ZnO-based sensors can also be promoted by the addition of small amounts of various metals such as Pt, Pd, and Ag. The metal additives affect the sensor properties in a rather complex manner. The types of interactions between metal additive and oxide semiconductor have been conceived, as shown in Figure 4.6. For example, an inflammable gas (CO) is activated by the metal additive and the activated fragments (CO) of the gas are spilt-over to the semiconductor surface to react with the adsorbed oxygen. The metal additive thus facilitates chemical reaction of the gas on the semiconductor. This type of promoting effect is called chemical sensitization. The spillover phenomenon is known to occur in the catalysis of metal loaded oxides so that this type of sensitization has been assumed for metal-loaded sensors. Thus leads to an increase in concentration of electrons [18].
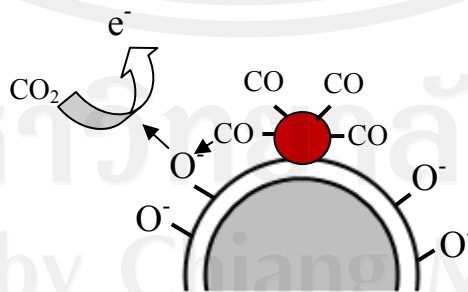
Figure 4.6 Mechanism of sensitization by metal additive [18].

4.1.6   Literature review

Pure and metal-doped ZnO gas sensing properties have been investigated by many researchers as shown in Tables 4.1.

Table 4.1 A summary on the gas sensing properties of pure/doped metal oxide semiconductors for NO_2, CO, C_2H_5OH and acetone gas.

Authors	Preparation of sensors	Thickness of Films	Loading level	Gas Concentration	Operating Temperature	Response (%)	Response Time	Recovery Time
Oh et al., 2009 [27]	RF sputtering technique	40 nm	Pure ZnO ZnO nanorod	10 ppb NO_2	250°C	37	4.5 min.	4 min.
Shouli et al., 2010 [28]	low temperature hydrothermal process	-	Pencil-like ZnO nanorods	40 ppm NO_2	400°C	239.5	-	-
	low temperature hydrothermal process	-	Pencil-like ZnO nanorods	400 ppm Ethanol	350°C	214.9	-	-
	low temperature hydrothermal process	-	Pencil-like ZnO nanorods	400 ppm acetone	400°C	118.3	-	-
	sol-hydrothermal process	-	Flower-like ZnO crystals	40 ppm CO	400°C	69.76	-	-
	low temperature hydrothermal process	-	5 wt% Cd/ZnO	40 ppm NO_2	400°C	470	-	-
	low temperature hydrothermal process	-	5 wt% Cd/ZnO	40 ppm CO	400°C	169.2	-	-

Authors	Preparation of sensors	Thickness of Films	Loading level	Gas Concentration	Operating Temperature	Response (%)	Response Time (min.)	Recovery Time (min.)
Calestani et al., 2010 [29]	Combination of thermal evaporation	50–200 nm	ZnO tetrapods	20 ppm NO_2	300°C	~20	-	-
				50 ppm Ethanol	300°C	~20	-	-
				10 ppm CO	300°C	< 0.2	-	-
Ferro et al., 2006 [30]	Sprayed	60 nm	3 wt% In/ZnO	5 ppm NO_2	275°C	~54	-	-
			1 wt% In/ZnO	5 ppm NO_2	275°C	~49	-	-
Tamaekong et al., 2010 [31]	Spin-coated	15 μm	0.2 at.% Pt/ZnO	1000 ppm CO	350°C	2.9	10 s	10 s
Chang et al., 2008 [32]	Zinc metal powder grown on substrate [Immersed in ethanol: $HAuCl_4 \cdot 4H_2O$ sol[1]]	-	ZnO nanowires with Au	100 ppm CO	350°C	53	-	-
			ZnO nanowires with Au	50 ppm CO	250°C	60	-	-
	RF magnetron sputtering		Ga/ZnO film with Au	100 ppm CO	350°C	2.1	-	-
Shishiyanu et al., 2005 [33]	Ionic layer adsorption and reaction (SILAR)	-	5 at% Sn/ZnO film	1.5 ppm NO_2	150°C	11	-	-

Authors	Preparation of sensors	Thickness of Films	Loading level	Gas Concentration	Operating Temperature	Response (%)	Response Time (min.)	Recovery Time (min.)
Tamaekong et al., 2010 [34]	Spin-coated	-	Pure ZnO	50 ppm NO_2 50 ppm Ethanol	300°C	33 7	7 94	- -
Sahay et al., 2005 [35]	The sprayed film	~ 20 nm	Pure ZnO	1000 ppm Ethanol	350°C	~11	2	1.5
Liewhiran al., 2007 [36]	Spin-coated	5µm	1mol%Pd/ZnO films	250 ppm Ethanol	400 °C	65.7	15s	-
Hongsith et al., 2008 [37]	Applying silver electrode at each end of the tube	-	1wt% Au/ZnO nanowires films	1,000 ppm Ethanol	240°C	37	-	-
Shishiyanu et al., 2005 [38]	Successive ionic layer adsorption and reaction (SILAR)	-	10 at% Sn/ZnO film	1.5 ppm NO_2	150°C	1.5-1.8	-	60

Oh et al. [27] fabricated ZnO nanorod array sensor that can sense NO_2 gas (Fig 4.7). It was found that ZnO-based NO_2 gas sensor showed the lowest detection limit of 10 ppb with short response and recovery time.
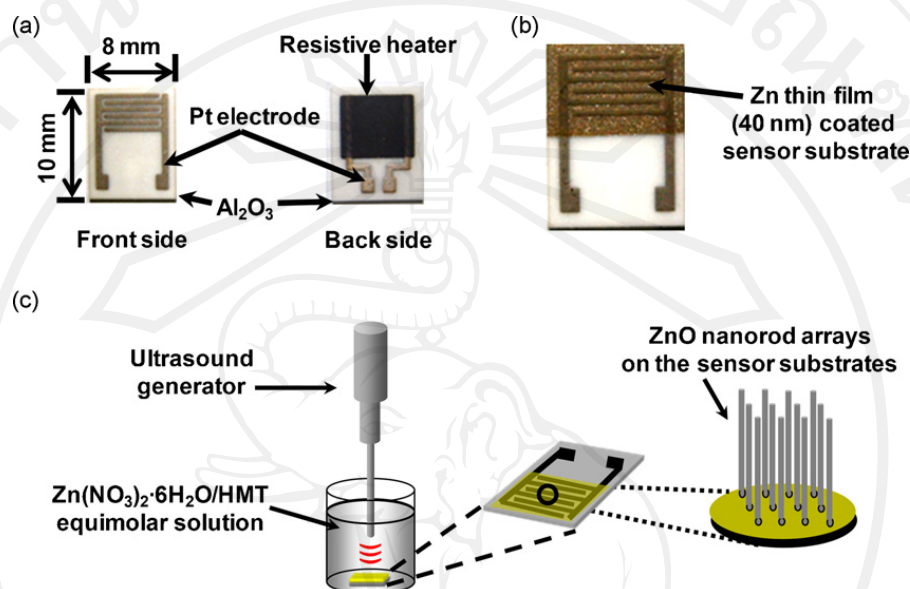
Figure 4.7 (a) Photograph of sensor substrate including interdigitated comb-like Pt electrodes and a resistive heater. (b) Zn thin-film sputtered sensor substrate. (c) A schematic illustration for the sonochemical growth of vertically aligned ZnO nanorod arrays on a sensor substrate.

Shouli et al. [28] synthesized three different morphologies of 1D ZnO nanocrystals by low temperature hydrothermal process and sol-hydrothermal process. The experimental results demonstrate that surfactant was very important in controlling the morphology of the nanocrystals. The morphology and sensing property of ZnO nanocrystals obtained by different synthesis methods were compared, it was found that the pencil-like ZnO nanorods synthesized by CTAB-assisted low temperature hydrothermal process had a good response towards 40 ppm NO_2 as high as 239.5 at the operating temperature of 400ºC. While flower-like ZnO crystals synthesized by

hydrothermal process exhibited good response of 69.76 to CO. The responses towards NO_2 and CO were greatly enhanced from 239.5 to 470.0 and from 52.2 to 169.2, respectively, by the addition of 5 wt% Cd as dopants during CTAB-assisted low temperature hydrothermal process.

Standard vapour phase growth process for ZnO tetrapods was optimized in order to reach a very large yield, a good reproducibility and a single morphology by Calestani et al. [29] The large yield of the growth and the simple deposition of these nanostructures on an alumina substrate with contacts and heater, allowed us to realize gas sensor prototypes with a relatively low-cost procedure. Good responses were observed towards NO_2 and CH_3CH_2OH (S≈20 for 20ppm of NO_2 and 50 ppm of CH_3CH_2OH), while lower values were obtained towards CO (S < 0.2 for 10 ppm of CO).

The effect of In-doping on the sensor performance was studied by Ferro et al. [30] With the addition of 1 and 3 wt% of indium nitrate to the spraying solution, a good sensor response to 5 ppm of NO_2 at 275ºC and an important decrease in the device electrical resistance is obtained.

Tamaekong et al. [31] produced ZnO nanoparticles doped with 0.2–2.0 at% Pt in a single step by FSP technique using zinc naphthenate and platinum (II) acetylacetonate dissolved in xylene. The gas sensing properties towards carbon monoxide (CO) was studied at the operating temperatures ranging from 200 to 350ºC. It was found that the 0.2 at% Pt/ZnO sensing film showed the highest sensitivity and the fastest response time at 350ºC.

Chang et al. [32] report the growth of high density single crystalline ZnO nanowires on patterned ZnO:Ga/SiO$_2$/Si templates, adsorption of Au nanoparticles on

nanowire surfaces and the fabrication of ZnO nanowire-based CO gas sensors. It was found that the device sensitivities were significantly enhanced by Au adsorption. With Au adsorption, it was also found that large (60%) sensitivity could be achieved at 250°C. Furthermore, it was found that the response speed and stability of the fabricated sensor were both good.

Shishiyanu et al. [33] fabricated NO_2 gas sensor by successive ionic layer adsorption and reaction (SILAR) technique of the Sn-doped ZnO film. The experimental results showed that tin doping of zinc oxide thin films improved the sensor element sensitivity to 1.5 ppm NO_2 in air and downshifted the operating temperature. The composition of 5 at% Sn in ZnO thin film shows a maximum sensitivity of 11 at 150ºC and a sensitivity of 1.5−2.0 at room temperature (25ºC) towards 1.5 ppm of NO_2 gas. There was a decrease of sensitivity when the operating temperature becomes higher than 250ºC. A composition of 10 at% Sn in ZnO thin film shows a maximum sensitivity of about 6 at 150ºC and a sensitivity of 1.5−1.8 at room temperature (25ºC) toward 1.5 ppm of NO_2 gas in air.

Using zinc naphthenate dissolved in xylene as a precursor undoped ZnO nanopowders were synthesized by the flame spray pyrolysis technique was reported by Tamaekong et al. [34]. The gas sensitivity of the undoped ZnO nanopowders towards 50 ppm of NO_2, C_2H_5OH and SO_2 were found to be 33, 7 and 3, respectively. The sensors showed a great selectivity towards NO_2 at high working temperature (at 300°C), while small resistance variations were observed for C_2H_5OH and SO_2, respectively.

Sahay et al. [35] reported on the details of preparing of ZnO thin films by spray pyrolysis and the sensing behaviors of the films to ethanol. The sprayed ZnO

thin films showed considerable changes in their resistances when exposed to ethanol with different temperature. It was found that the film layers of 20 μm in thickness showed sensitivity in terms of rather high ethanol concentration (1000–5000 ppm) at 150–350°C. It was observed that the sensitivity increased with increasing operating temperature. At higher ethanol concentration, the sensitivity increased rapidly with increasing operating temperature. Response and recovery times were found to be sensitively dependent upon the operating temperature.

Liewhiran and Phanichphant [36] reported the effect of Pd loading on the ethanol gas sensing performance of the ZnO nanoparticles and the crystalline sizes. In the experiment, ZnO nanoparticles doped with 0–5 mol% Pd were successfully produced in a single step by FSP using zinc naphthenate and palladium (II) acetylacetonate dissolved in toluene-acetonitrile (80:20 vol%) as precursors. The gas sensing of ethanol (25–250 ppm) was studied in dry air at 400°C. The oxidation of ethanol on the sensing surface of the semiconductor was confirmed by Mass spectroscopy (MS). A well-dispersed of 1 mol% Pd-doped ZnO films showed the highest sensitivity and the fastest response time (within seconds).

ZnO nanowires and Au-doped ZnO nanowires were prepared by oxidation reaction reported by Hongsith et al. [37]. The oxidation was performed by heating zinc powder (purity 99.9%) with a mixture of zinc powder and 1 wt% gold powder. The pressed powders were sintered at 600 ºC for 24h. The ZnO nanowires and the Au-doped ZnO nanowires were characterized using field emission scanning electron microscopy (FE-SEM) and EDS to examine morphology and composition, respectively. The ethanol sensing properties of ZnO nanowires were observed from the resistance change under ethanol vapor atmosphere, for ethanol concentrations of

100, 500, 1,000 and 2,000 ppm, and at operating temperatures of 180–280 ºC. It was found that the nanowires and the Au-doped ZnO nanowires had diameters between 60 and 180 nm respectively and lengths of about 5–10 μm. This suggested that the addition of 1 wt% Au dopant had no effect on the morphology of ZnO nanowire. The sensitivity of both ZnO nanowire and Au-doped ZnO-nanowire sensors depended on the operating temperature at each ethanol concentration The optimum operating temperature was at 240ºC with the highest sensitivity of 27 for ZnO-nanowire sensors and 37 for Au-doped ZnO-nanowire sensors. The sensitivity of the sensor based on Au-doped ZnO nanowires exhibited higher values than that of the sensor based on undoped ZnO nanowires. This suggested that the Au-doping on ZnO nanowires has enhanced the performance of the ethanol sensor.

The sensitivity of zinc oxide films doped with Sn, Cu, Al and Pd grown by SILAR method and rapid photothermal processed were studied bv Sergiu et al. [38]. The experimental results showed that tin doping of zinc oxide thin films improved the sensor element sensitivity to 1.5 ppm NO_2 in air and downshifted the operating temperature. The sensitivity of Sn-doped zinc oxide-based sensor to NO_2 was higher than that of Cu, Al and Pd-doped ZnO films for all the concentrations studied at room temperature and 150ºC. The Sn-ZnO sensor element had a fast response time and higher sensitivity compared to Cu-ZnO and Pd-doped ZnO-based elements. The obtained experimental results showed that increasing the Sn concentration from 5 to 10 at% in the ZnO film led to the sensitivity decrease of the sensor element and increase the response time. The sensitivity of Sn-doped zinc oxide-based gas sensor element towards 1.5 ppm of NO_2 versus the operating temperature. The composition of 5 at% Sn in ZnO thin film showed a maximum sensitivity of 11 at 150ºC and a

sensitivity of 1.5-2 at room temperature 25ºC toward 1.5 ppm of NO_2 gas. There was a decrease of sensitivity when the operating temperature became higher than 250ºC. A composition of 10 at% Sn in ZnO thin film shows a maximum sensitivity of about 6 at 150ºC and a sensitivity of 1.5-1.8 at room temperature (25ºC) towards 1.5 ppm of NO_2 gas in air.

4.2   Chemicals and equipments

- Pure ZnO and Nb-doped ZnO nanoparticles

- Ethyl cellulose (Fluka, 30-60 mPa.s)

- Terpineol (Aldrich, 90%)

- Al_2O_3 substrates interdigitated with Au electrodes (Au/Al_2O_3; 0.5x 0.24

    cm; National Electronics and Computer Technology Center, Thailand)

    Spin coater (Laurell, WS-400B-6NPP-LITE)

- Three-zone tube furnace (Lenton, PTF 15)

- Lab-set gas sensor measurement (National Electronics and Computer

    Technology Center, Thailand)

- Scanning electron microscope & EDS (JSM-6335F, JEOL)

4.3   Experimental

4.3.1   Sensing film fabrication

Sensing films were prepared using flame-made pure ZnO, 0.25 mol% Nb-doped ZnO, 0.50 mol% Nb-doped ZnO and 1.00 mol% Nb-doped ZnO by mixing 60 mg of the nanoparticles into an organic paste composed of ethyl cellulose (Fluka, Viscosity: 30–70 mPa·s at 25°C) and terpineol (Aldrich, 90%), which acted as a vehicle binder and solvent, respectively. Figure 4.8(a) shows the sensor substrate,

illustrating interdigitated Au electrodes. The alumina substrate has a dimension of 0.4 cm × 0.55 cm × 0.04 cm and the interdigitated electrode area was 0.24 cm × 0.5 cm. 200 nm-thick Au layers were deposited by DC sputtering in argon gas at a pressure of 3×10^{-3} mbar. ZnO thin-film was deposited on the sensor substrate using spin coating. After ZnO thin-film (10 μm) deposition on the interdigitated Au electrodes as shown in Figure 4.8(b), the sensing films were then subsequently at 400°C for 2 h (with heating rate of 2 °C/min) for binder removal and finally cooled down to room temperature. The particle size of films was slightly changed after annealing.
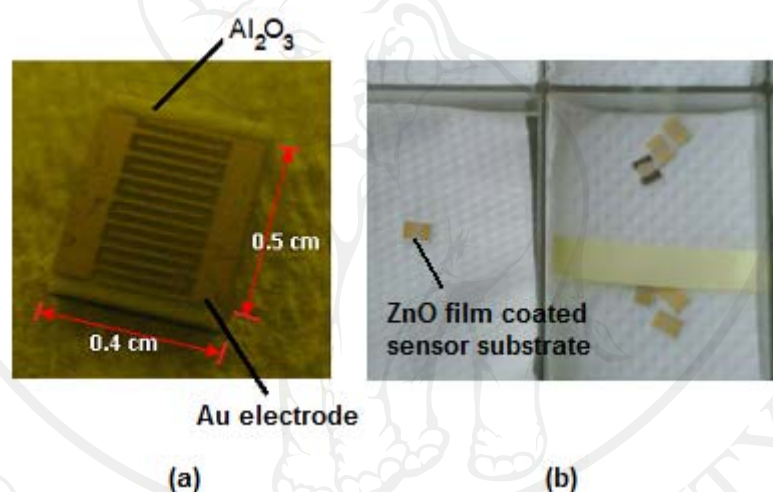
Figure 4.8 (a) Photograph of sensor substrate including interdigitated comb-like Au electrodes. (b) ZnO thick-film spin coat sensor substrate.

4.3.2 Sensing film characterization

The morphologies, cross section and elemental compositions of sensing films were analyzed by SEM and EDS line-scan mode analyses.

4.3.3 Gas sensing characterization

The sensor characteristics of metal oxide nanoparticles were characterized towards the low dynamic range in concentration of NO_2 (0.1–4 ppm) and high

dynamic range in concentration of C_2H_5OH, CO and H_2 (50−1000 ppm). The flow through technique was used to test the gas-sensing properties of thin films. A constant flux of synthetic air of 2 l/min was mixed with the desired concentrations of pollutants. All measurements were conducted in a temperature-stabilized sealed chamber at 20^oC in the presence of dry air. The external NiCr heater was heated by a regulated dc power supply to different operating temperatures. The operating temperature was varied from 250^oC to 350^oC. The resistances of various sensors were continuously monitored with a computer-controlled system by voltage-amperometric technique with 5 V dc bias and current measurement through a picoammeter. The sensor was exposed to a gas sample for ~10 minutes for each gas concentration testing and then the air flux was restored for 30 minutes. The NO_2 concentration was varied from 0.1−4 ppm of concentration and C_2H_5OH, CO and H_2 were varied from 50−1000 ppm of concentration. Figure 4.9 showed the experimental set up for gas sensing test.
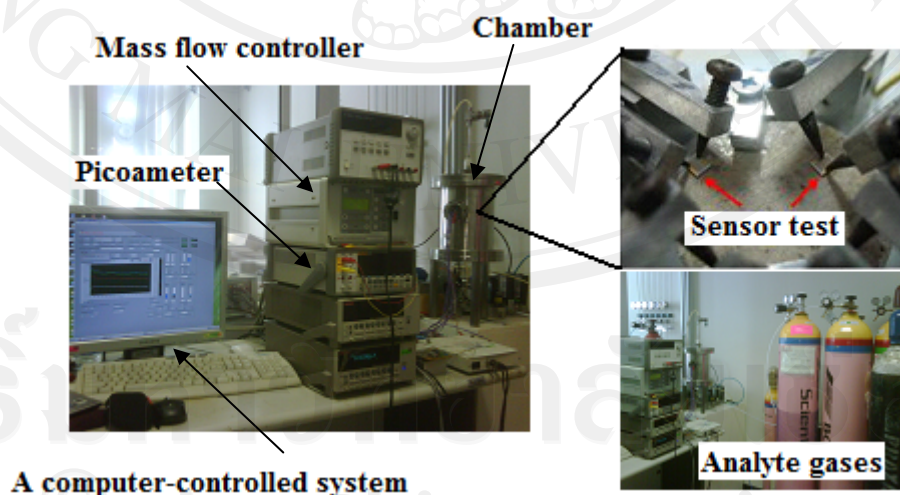
Figure 4.9 Gas sensor measurement setup.

4.4   Results and discussion

4.4.1   Sensing film properties

4.4.1.1 X-ray diffraction analysis

Gas sensing films based on flame-made pure ZnO and 0.25–1.00 mol% Nb-doped ZnO nanoparticles after anneal and sensing test at 350ºC were analyzed by X-ray diffraction spectroscopy (XRD, Philip X' Pert PRO PW 3719) using CuK$_\alpha$ radiation at 2θ = 20-80º with a step size of 0.06º and a scanning speed of 0.72º/min. The XRD patterns showed that the sensing films were highly crystalline, and all peaks can be confirmed to be the hexagonal structure of (●) ZnO match well with the JCPDS No. 89-0510 [39] (Figure 4.10). The XRD diffraction patterns from sensing film coated on Au/Al$_2$O$_3$ substrates showed that the diffraction patterns of (▲) Al$_2$O$_3$ (JCPDS file No. 82-1468 [40]) and (■) Au (JCPDS file No. 04-0784 [41]) from the substrates are also visible in these samples. Amorphous phase of ZnO and Nb peaks were not found in these patterns. It can be assumed that concentrations of Nb were very low and the sizes of Nb particles were too small to be detected by XRD.
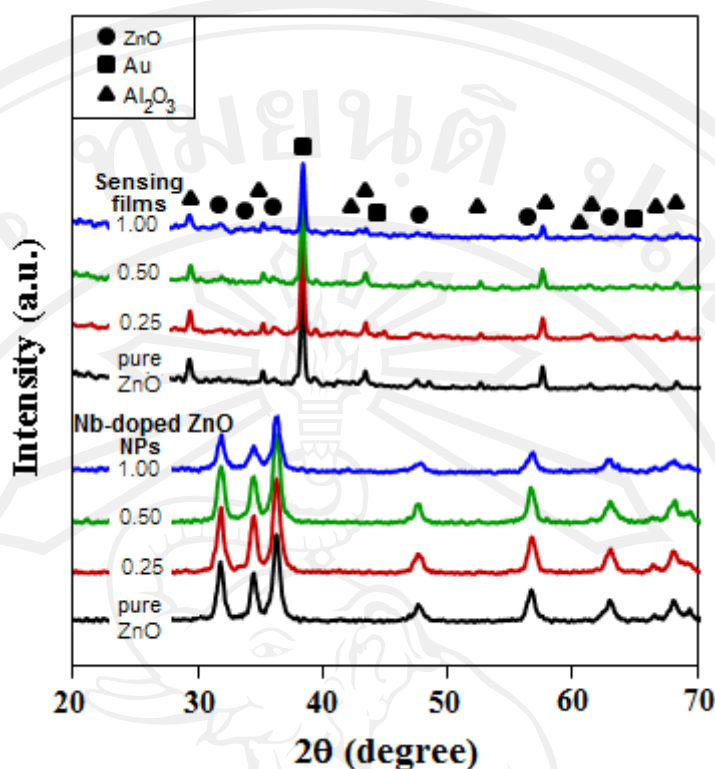
Figure 4.10 XRD patterns of the flame-made (5/5) pure ZnO and Nb-doped ZnO nanoparticles with different Nb concentrations, and samples of sensing films were spin-coated on Au/Al$_2$O$_3$ substrate after annealing and sensing test at 350°C. JCPDS files No. 89-0510, 04-0784 and 82-1468 as refer to (●) ZnO, (■) Au and (▲) Al$_2$O$_3$, respectively.

4.4.1.2 SEM-film thickness sensing layer

Figure 4.11 shows the SEM cross-section image of flame-spray-made of pure ZnO and 0.25, 0.50 and 1.00 mol% Nb-doped ZnO thick films at different magnifications on an Al$_2$O$_3$ substrate interdigitated with Au electrodes after annealing and sensing test at 350°C in dry air. It was found that film thickness of pure ZnO and 0.25, 0.50 and 1.00 mol% Nb-doped ZnO sensors were 10.5, 10.3, 9.5 and 9.1 μm, respectively.
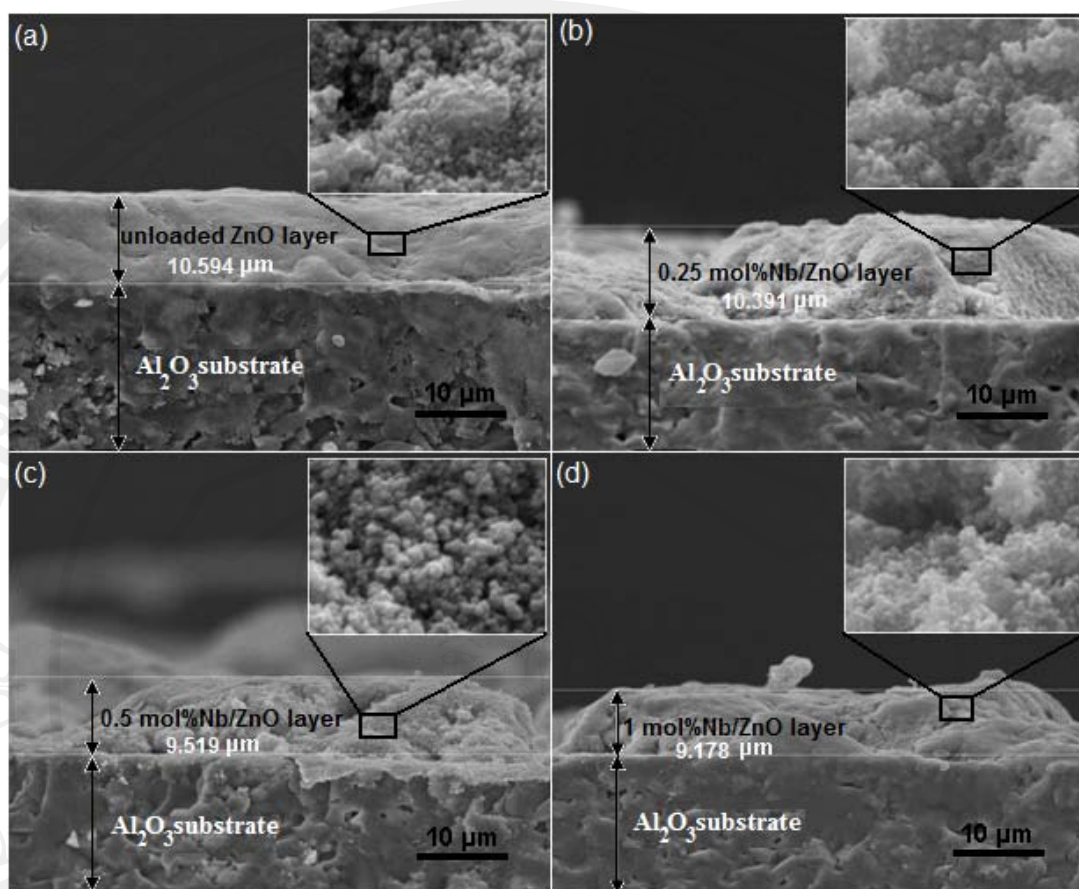
Figure 4.11 SEM micrographs of flame-made ZnO thick films as a sensor (a) pure ZnO, (b) 0.25 (C) 0.50 and (d) 1.00 mol% Nb-doped ZnO on an Al_2O_3 substrate interdigitated with Au electrodes after annealing and sensing test at 300°C in dry air. The film thickness was approximately 10 μm.

4.4.1.3 Energy Dispersive X-ray Spectrometry (EDS): line scan mode

The trends in the elemental composition of the agglomerated nanoparticles formed of pure ZnO and 0.25, 0.50 and 1.00 mol% Nb-doped ZnO was shown by the EDS line scan mode in Figures 4.12–4.15. Interestingly, the analyzed regions composed of the nanoparticles and gold sputtering prior to an analysis. The line scan across the agglomerate for the sensing films of pure ZnO and 0.25, 0.50 and 1.00 mol% Nb-doped ZnO are indicated in Figures 4.12–4.15. The elemental-line histograms were shown as signals corresponding to a rich in aluminum (Al) caused by

the contamination of alumina substrate, gold (Au), zinc (Zn), oxygen (O), and niobium (Nb) elements. After annealing process, a denser film layer was formed. Regularities and preciseness in the film thickness were affected from the spin coating technique.
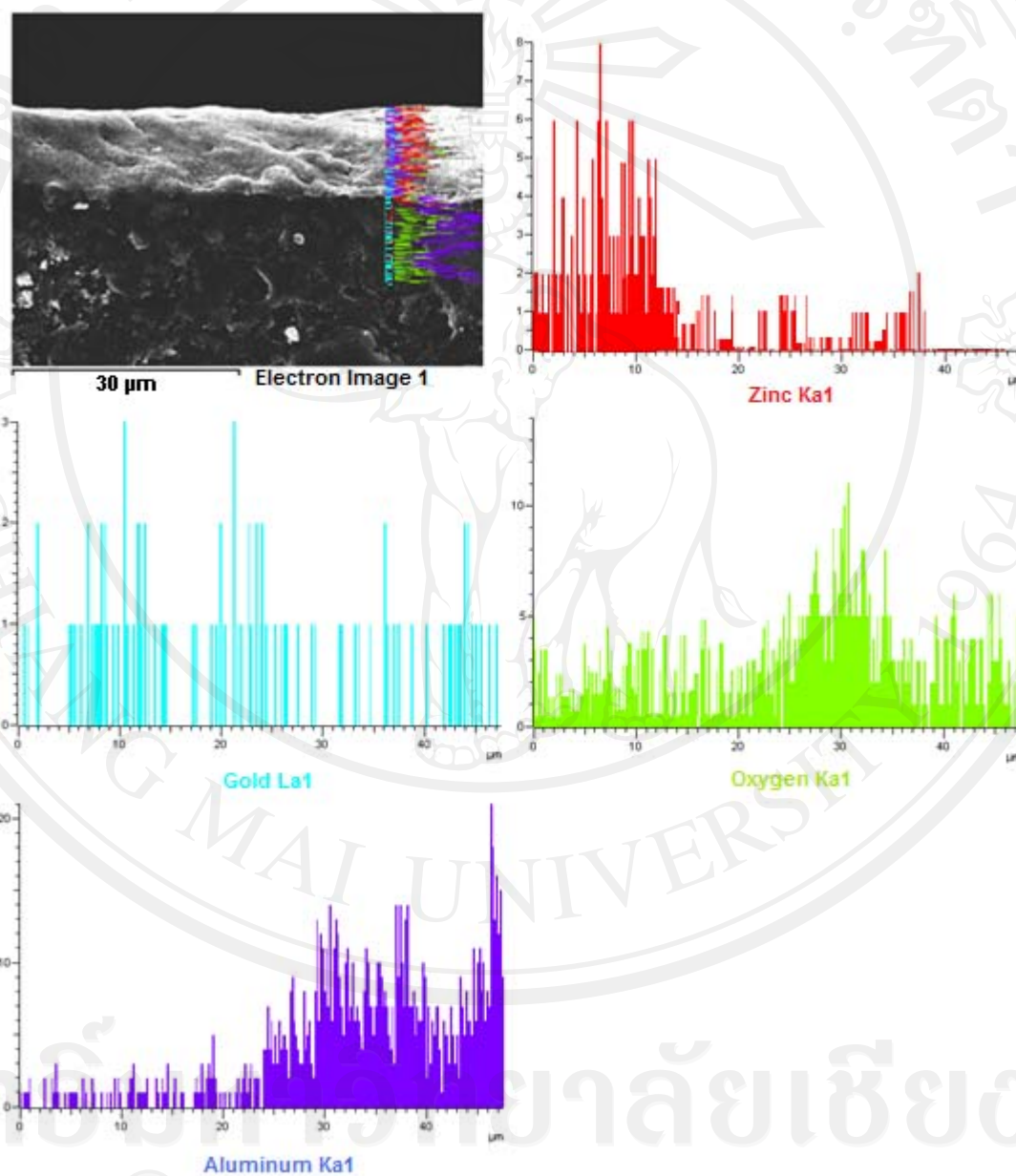
Figure 4.12 The EDS line scan mode of sensor based on flame-made pure ZnO nanoarticles. The histograms showed the elemental compositions of samples. The lines scans correspond to O, Zn, Al and Au elements.
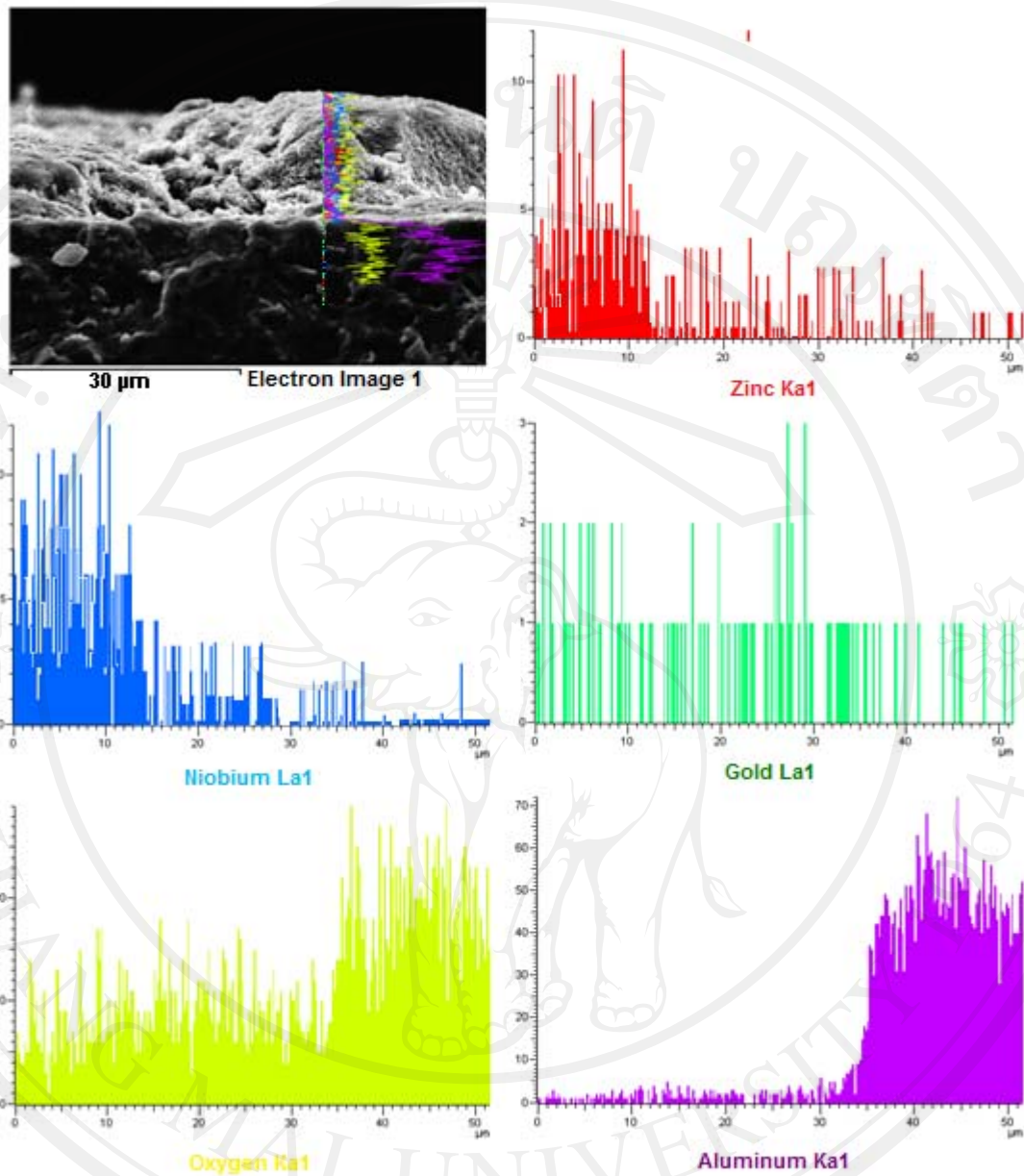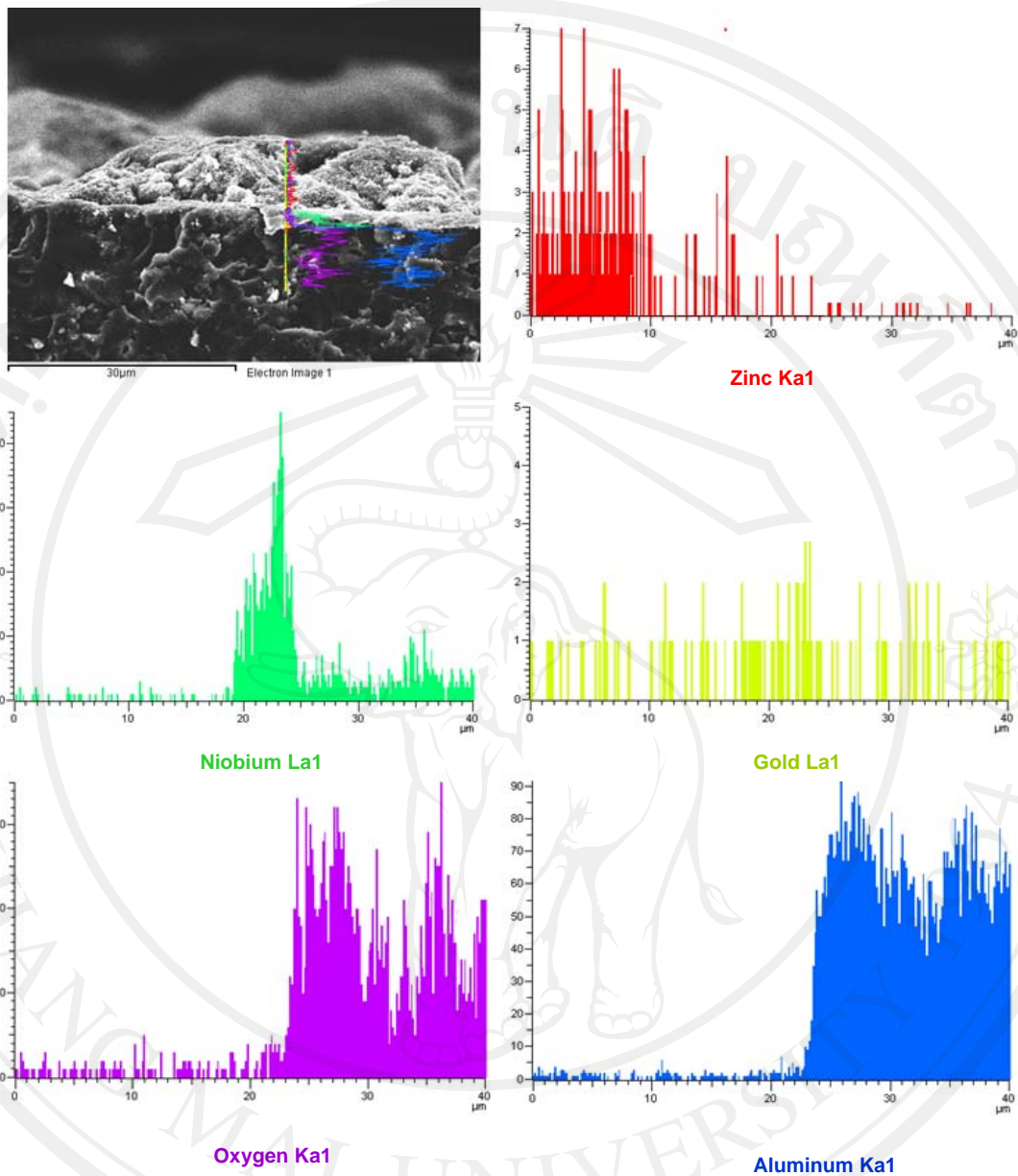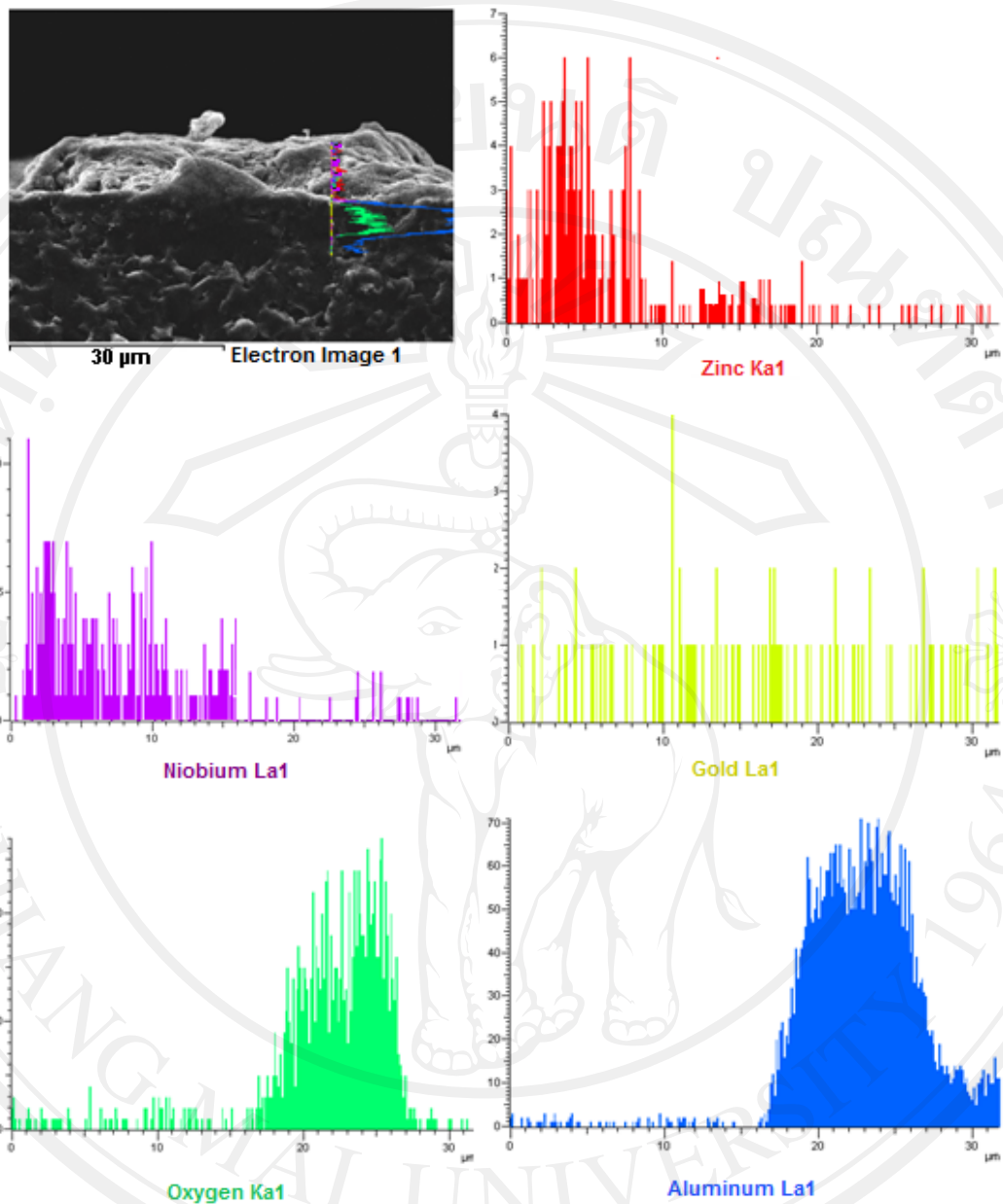
Figure 4.13   The EDS line scan mode of sensor based on flame-made 0.25 mol% Nb-doped ZnO nanoarticles. The histograms showed the elemental compositions of samples. The lines scans correspond to O, Zn, Al, Au and Nb elements.

Figure 4.14 The EDS line scan mode of sensor based on flame-made 0.50 mol% Nb-doped ZnO nanoarticles. The histograms showed the elemental compositions of samples. The lines scans correspond to O, Zn, Al, Au and Nb elements.

174

Figure 4.15   The EDS line scan mode of sensor based on flame-made 1.00 mol%
Nb-doped ZnO nanoarticles. The histograms showed the elemental compositions of
samples. The lines scans correspond to O, Zn, Al, Au and Nb elements.

4.4.2 Gas sensing properties

The dynamic changes of resistance to NO_2 (0.1–4 ppm) of ZnO films with difference Nb contents at operating temperature of 250ºC, 300ºC and 350ºC are shown in Figures 4.16–4.18. It can be seen that the resistant of all ZnO sensors increased upon the exposure to NO_2 which is an oxidizing gas, indicating that both the pure ZnO and Nb-doped ZnO films show the typical n-type semiconductor behavior. Comparing to pure ZnO film, all Nb-doped ZnO films had much higher resistance when exposed to NO_2. In addition 0.50 mol% Nb-doped ZnO film showed the highest response to NO_2. These results could be assumed that the gas sensing properties of ZnO nanoparticle films could be greatly improved by doping with an appropriate amount of Nb.
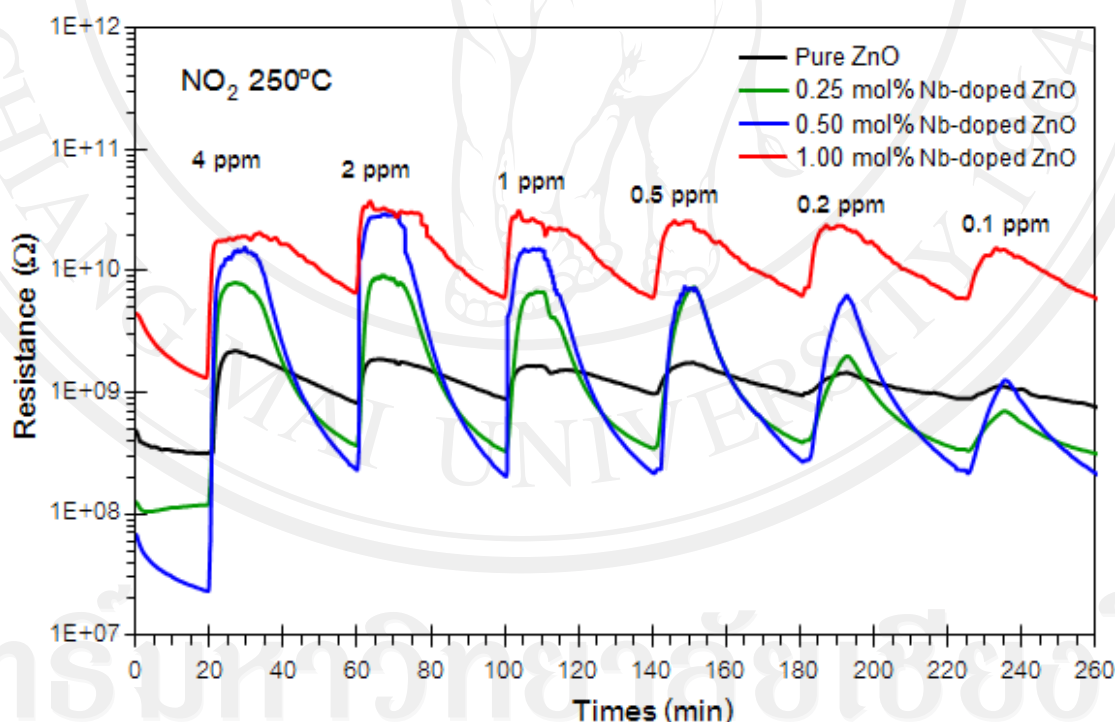
Figure 4.16 Dynamic response of pure ZnO and 0.25, 0.50 and 1.00 mol% Nb-doped ZnO gas sensor towards 0.1–4 ppm NO_2 gas square pulses at 250°C.
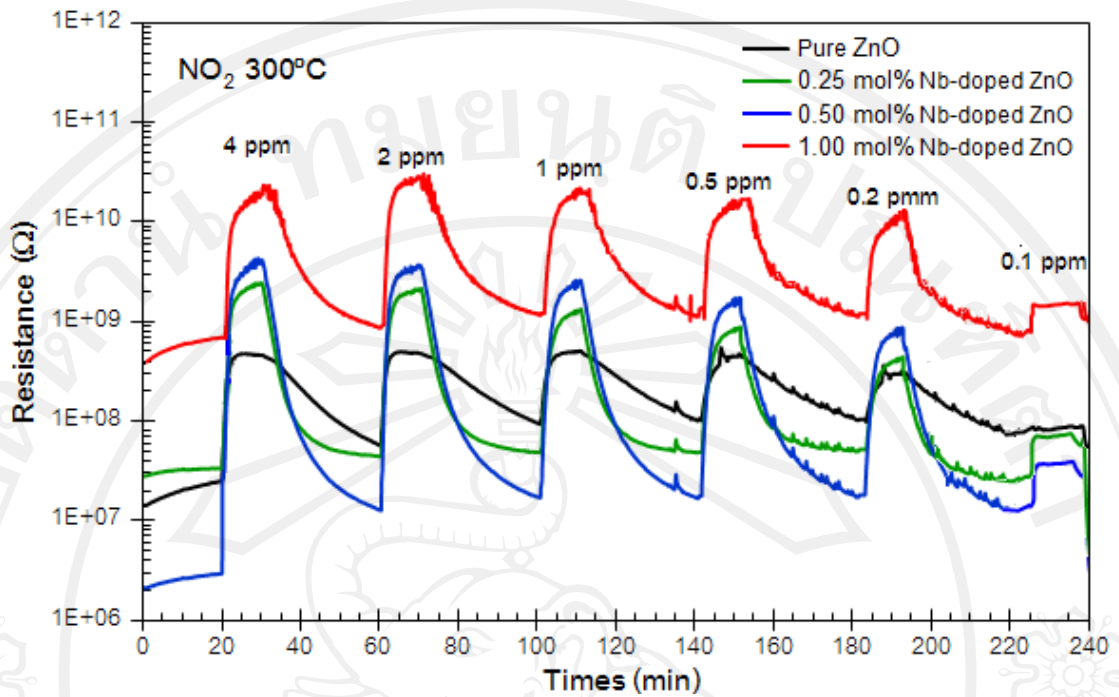
Figure 4.17 Dynamic responses of pure ZnO and 0.25, 0.50 and 1.00 mol%

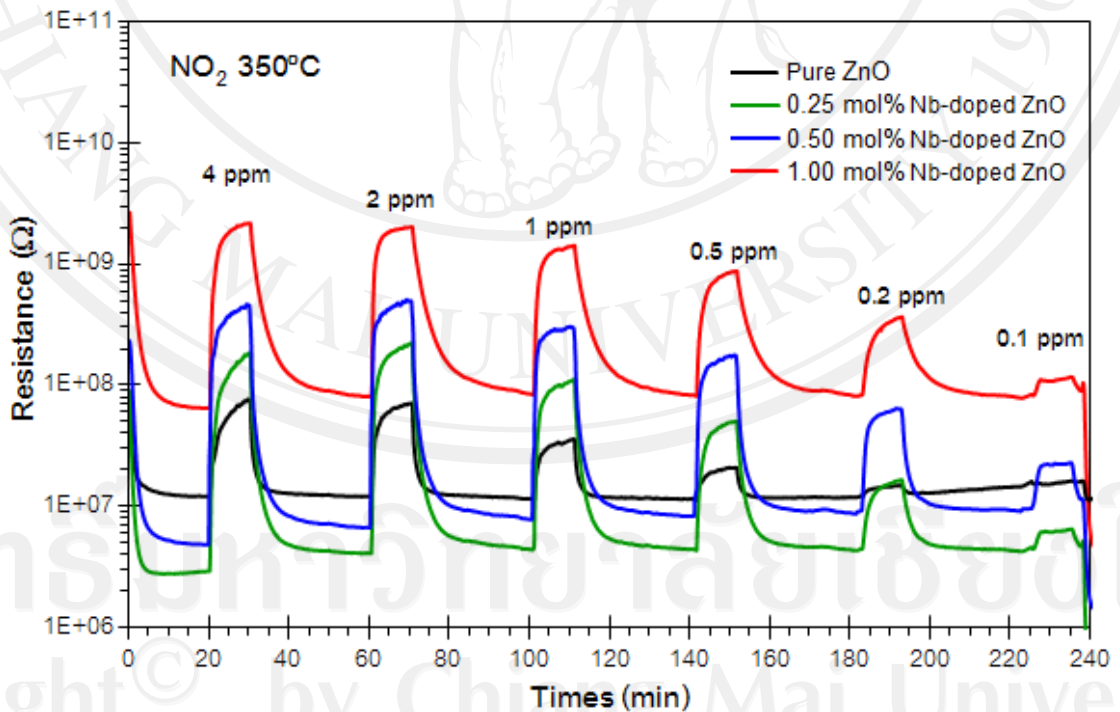Nb-doped ZnO gas sensor towards 0.1–4 ppm NO_2 gas square pulses at 300°C.

Figure 4.18 Dynamic response of pure ZnO and 0.25, 0.50 and 1.00 mol% Nb-

doped ZnO gas sensor towards 0.1–4 ppm NO_2 gas square pulses at 350°C.

From Figure 4.17 the sensors have acceptable reversibility. It is seen that the sensor resistance recovers to within 10% of its base line value after several NO_2 exposures. The deduced sensor response and response time are thus considered valid and meaningful. Nevertheless, it can be noticed that the sensors exhibit quite slow response and recovery of the order of minutes. This problem is due to the use of large-volume (5.2 L) test chamber and this can be solved by reducing the size of test chamber.

Figure 4.19 shows the effect of operating temperature on response with 4 ppm NO_2. The operating temperature dependence on the sensing properties could result from changing of the adsorption and desorption rates of the oxygen ions on the metal-oxide surface [42] (equations 4.10 and 4.11).

When the ZnO nanoparticles are exposed to NO_2 gas, NO_2 gas reacts with the adsorbed O^- ions as well as adsorbs directly on the surface of ZnO nanoparticles. Then, the concentration of electrons on the surface of ZnO nanoparticles arrays decreases and, correspondingly, the resistance of ZnO layer increases. The adsorption of O^- ions is very interesting step in metal-oxide gas sensor, because the O^- ions assist the adsorbed NO_2 ions to take the electrons from the ZnO nanoparticles arrays. The response of the ZnO sensor is relatively high due to adsorbed O^- ions at the temperature range of 250–350°C. As the temperature increases, however, the dominant process becomes the adsorption of O^- ions, then the response of the ZnO sensor decreases. Furthermore, progressive desorption of all species occurs and the response decreases at high temperature range. For these reasons, the response of ZnO sensor very steeply decreases at 350°C. It can be confirmed that the temperature dependence of sensor responses with different concentrations (0.1–4 ppm of NO_2

gases) showed a similar trend of maximum response at 300°C. The present results showed that the maximum response was obtained at a relatively low temperature of 300°C compared to the previous reports of 400°C [43–44].
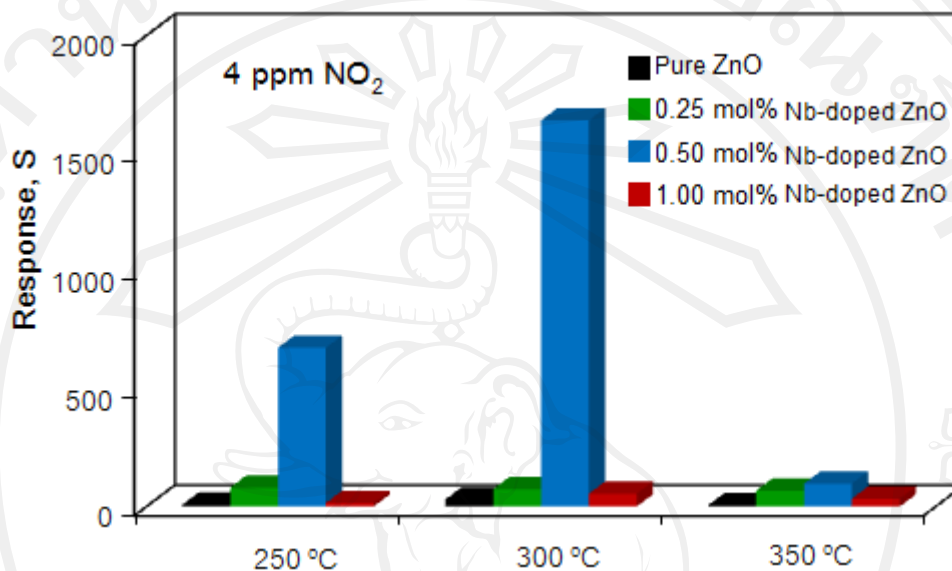

Figure 4.19 The response of Nb-doped ZnO gas sensor towards 4 ppm of NO_2 versus the operating temperature. The composition of 0.50 mol% Nb in ZnO thin film shows a maximum response of 1640 at 300°C.

The response and response time versus the NO_2 concentrations ranging from 0.1–4 ppm concentration based on ZnO nanoparticles at operating temperature of 300°C are shown in Figure 4.20. It can be seen that the semiconducting and gas-sensing behaviors are strongly depending on the Nb doping concentrations in ZnO nanoparticles. By doping ZnO nanoparticles with Nb, the NO_2 response was increased and response time was reduced. As the Nb doping concentration increases from 0 to 0.5 mol%, the response increases by more than two orders of magnitude and response time decrease by more than a factor of three. However, the response and response time are considerably degraded when the Nb doping concentration further increases from 0.5 to 1.0 mol%. Thus, the optimum Nb concentration was 0.5 mol%.

The detection range of 0.1–4 ppm of the Nb-doped ZnO nanoparticles is very important in the context of experimental pollution monitoring. According to U.S. Environmental Protection Agency (EPA) standard, the allowed NO_2 concentration in normal ambient air is 53 ppb (0.053 ppm) while the allowed NO_2 concentration at source is around 3 ppm. Thus, Nb-doped ZnO nanoparticles based sensors have promising performance of environmental monitoring of NO_2. The 0.5 mol% Nb-doped ZnO sensor gives a good sensitivity of ~5 at 100 ppb and minimum detection limit can be estimated to be 20 ppb (at a sensitivity of ~1.1). It should be noted that the lowest tested concentration is presently limited at 100 ppb due to the gas mixing capability of our system and this limit will be reduced by the use of lower concentration NO_2 standard gas in the future.
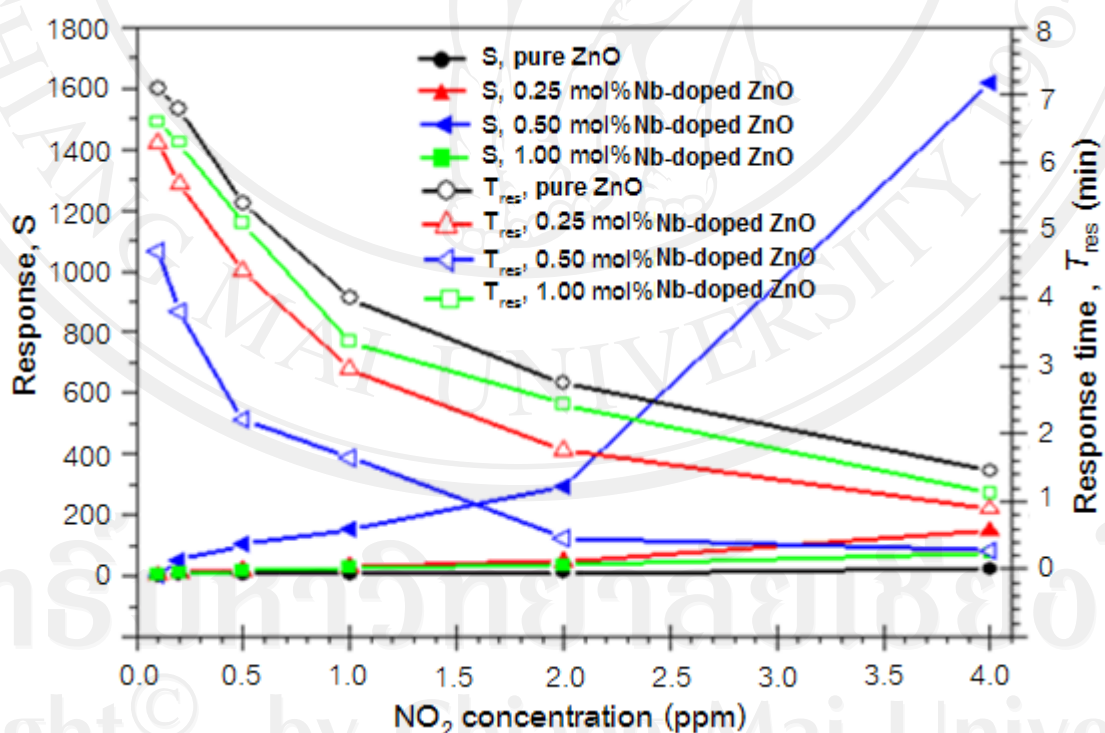

Figure 4.20 Variation of response (left) of NO2 concentrations (0.1–4 ppm) and variation of response times (right) with change in resistance at 300°C.

The dynamic changes of resistance to C_2H_5OH concentrations ranging from 50 –1000 ppm concentration based on ZnO films with difference Nb contents at operating temperature of 350ºC were shown in Figure 4.21 and the response were shown in Figure 4.22. It can be seen that the resistant of all ZnO sensors increased upon the exposure to NO_2 which is a reducing gas, indicating that both the pure ZnO and Nb-doped ZnO films show the typical n-type semiconductor behavior. Comparing to pure ZnO film, all Nb-doped ZnO films had much higher resistance when exposed to C_2H_5OH. In addition 0.50 mol% Nb-doped ZnO film showed the highest response towards C_2H_5OH.
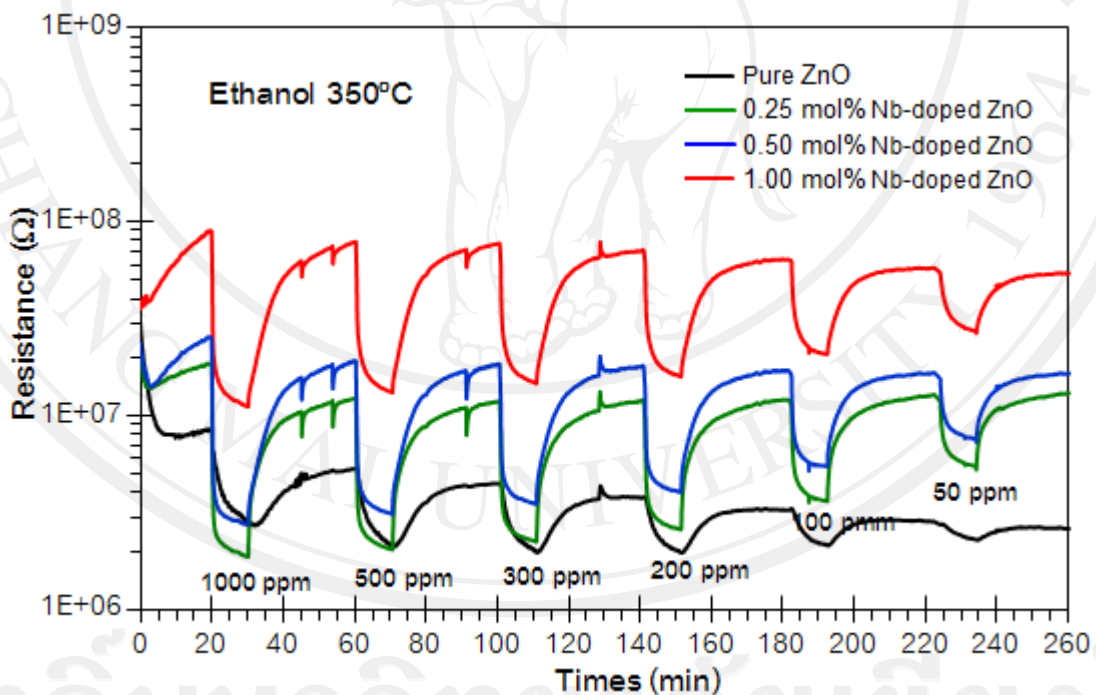

Figure 4.21 Dynamic response of pure ZnO and 0.25, 0.50 and 1.00 mol% Nb-doped ZnO gas sensor towards 50–1000 ppm C_2H_5OH gas square pulses at 350°C.
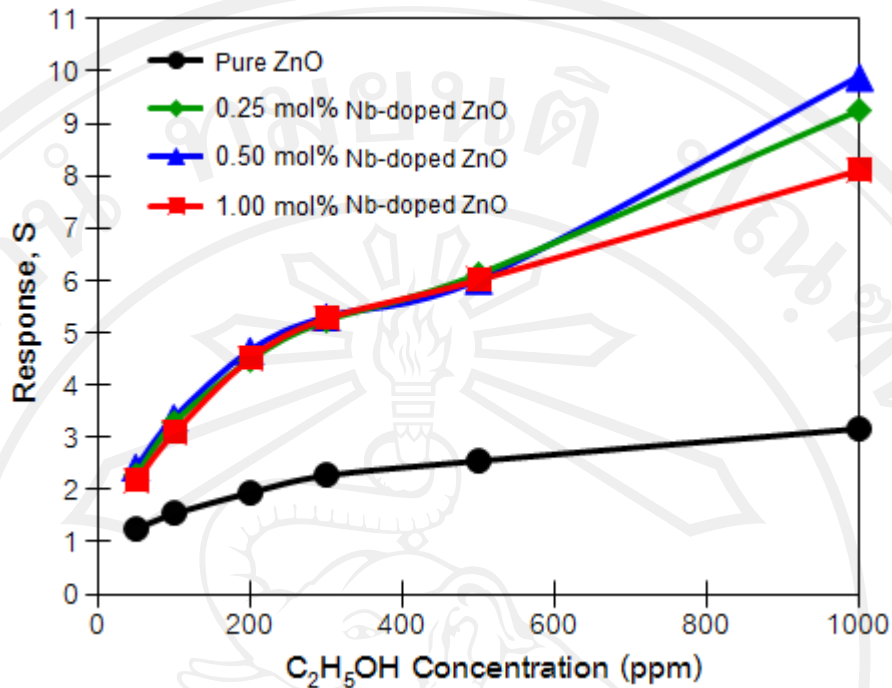
Figure 4.22 Variation of response of C_2H_5OH concentrations (50−1000 ppm) with change in resistance at $350^{\circ}C$.

The dynamic changes of resistance to acetone concentrations ranging from 50−1000 ppm concentration based on ZnO films with difference Nb contents at operating temperature of 350ºC are shown in Figure 4.23 and the response were shown in Figure 4.24. It can be seen that the resistant of all ZnO sensors increased upon the exposure to acetone which was a reducing gas, indicating that both the pure ZnO and Nb-doped ZnO films show the typical n-type semiconductor behavior. Comparing to pure ZnO film, all Nb-doped ZnO films had much higher resistance when exposed to acetone. In addition 0.50 mol% Nb-doped ZnO film showed the highest response towards acetone.
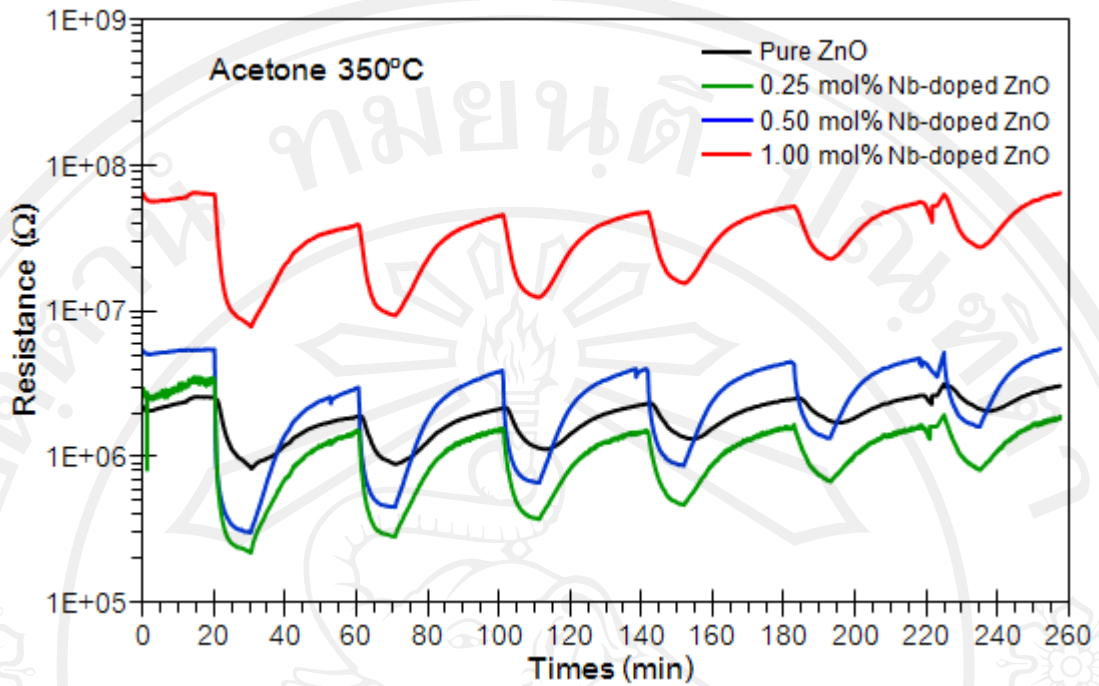
Figure 4.23 Dynamic response of pure ZnO and 0.25, 0.50 and 1.00 mol% Nb-doped ZnO gas sensor towards 50–1000 ppm acetone gas square pulses at 350°C.
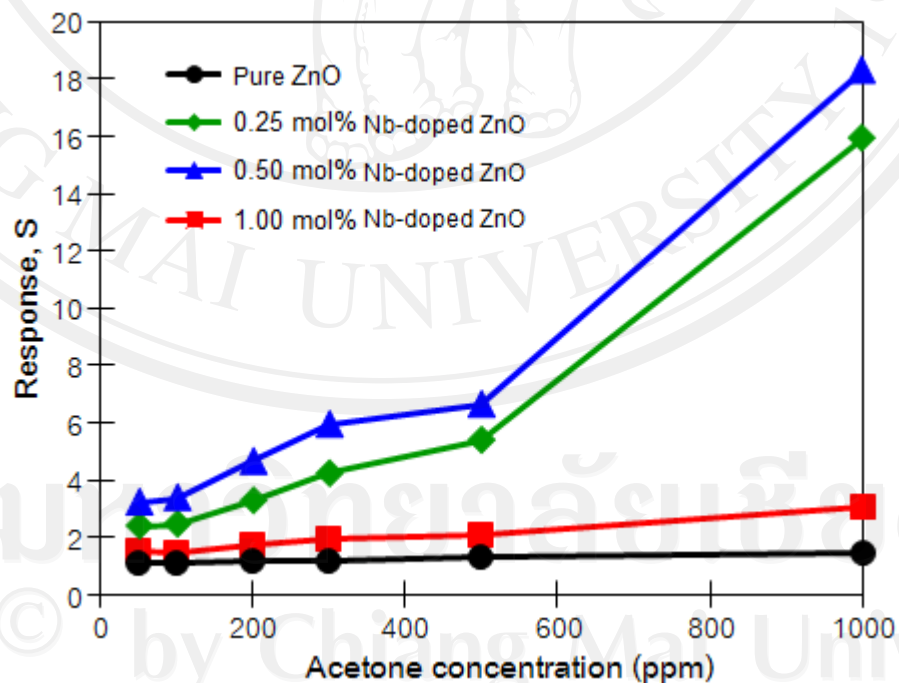

Figure 4.24 Variation of response of acetone concentrations (50–1000 ppm) with change in resistance at 350°C.

The dynamic changes of resistance to CO concentrations ranging from 50–1000 ppm concentration based on ZnO films with difference Nb contents at operating temperature of 350ºC are shown in Figure 4.25 and the response are shown in Figure 4.26. It can be seen that the resistant of all ZnO sensors increased upon the exposure to CO which is a reducing gas, indicating that both the undoped ZnO and Nb-doped ZnO films show the typical n-type semiconductor behavior. Comparing to pure ZnO film, all Nb-doped ZnO films had much higher resistance when exposed to CO. In addition 0.50 mol% Nb-doped ZnO film showed the highest response towards CO.
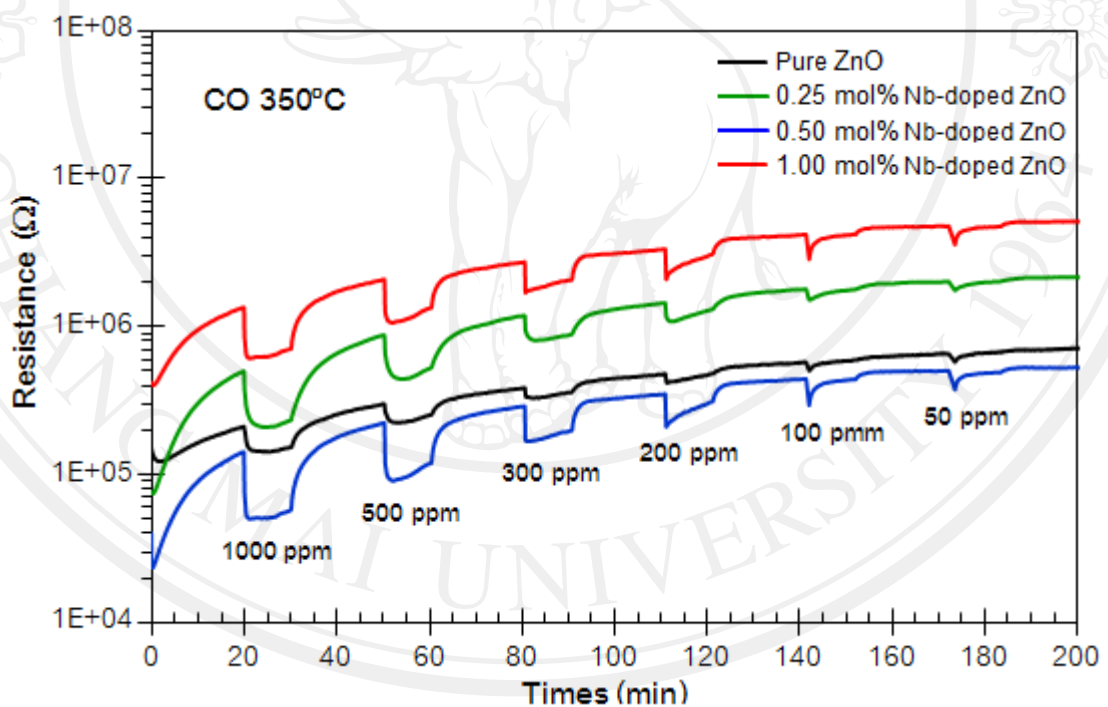

Figure 4.25 Dynamic response of pure ZnO and 0.25, 0.50 and 1.00 mol% Nb-doped ZnO gas sensor element from 50–1000 ppm CO gas square pulses at 350°C
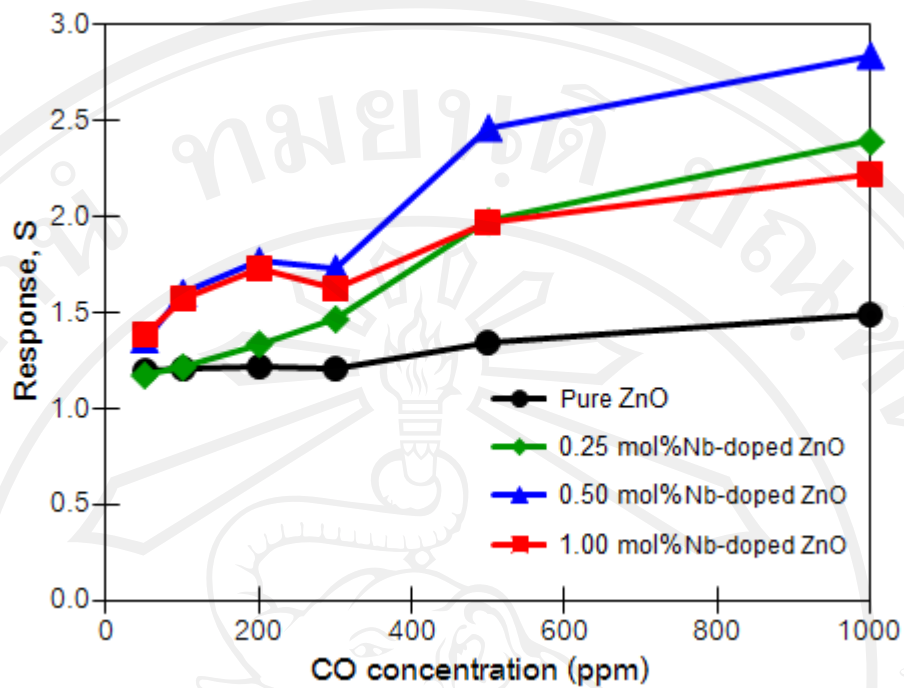
Figure 4.26 Variation of response of CO concentrations (50−1000 ppm) with change
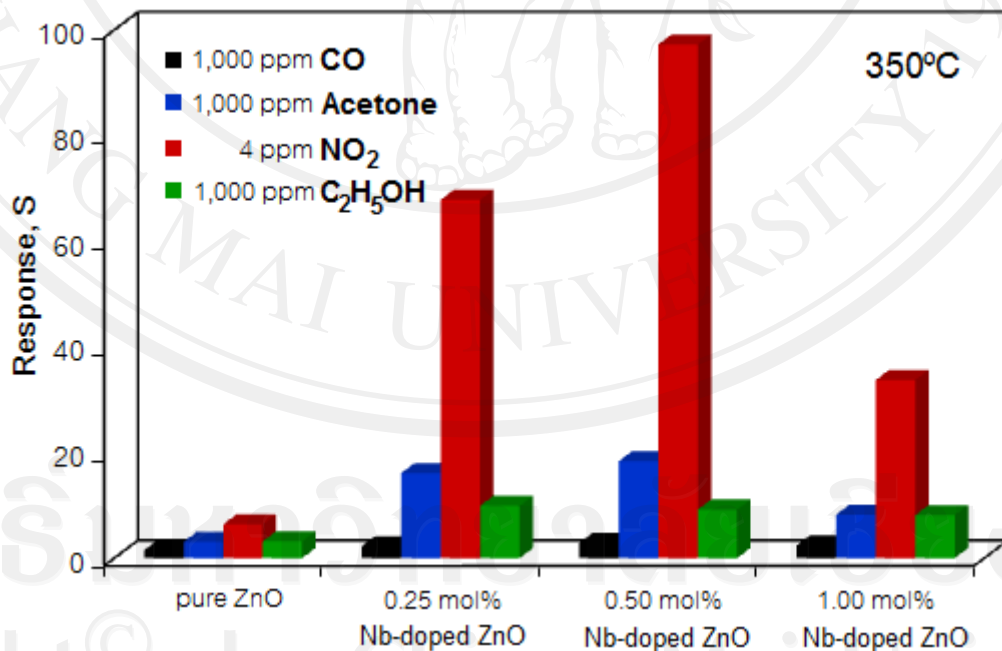
in resistance at 350°C.

Figure 4.27 Variation of response with concentration of NO_2 (4 ppm), CO, C_2H_5OH

and acetone (1000 ppm) at 350°C for sensor of pure ZnO as compared to 0.25, 0.50

and 1.00 mol% Nb-doped ZnO.

From Figure 4.27, 0.5 mol% Nb-doped ZnO gas sensor has good gas selectivity to 4 ppm of NO_2 concentration of 98.5 at 350^oC. The response of 0.5 mol% Nb-doped ZnO sensing films towards C_2H_5OH, CO and acetone were 9.1, 2.4 and 19.8 respectively at 0.1 vol% concentration at 350^oC. Therefore, 0.5 mol% Nb-doped ZnO gas sensor can be used for selective detection of these four gases. It should be noted that C_2H_5OH, acetone and CO are selected for selectivity study because they possess similar properties due to their comparable molecular weights (MW of acetone, NO_2, C_2H_5OH and CO are 58, 46, 46 and 28, respectively).

4.5   Conclusions

Pure ZnO and Nb-doped nanoparticles containing 0.25, 0.5 and 1 mol% Nb were produced in a single step by FSP technique. The sensor performance of spin coated ZnO thick film-based NO_2 sensor was enhanced by Nb-doping. ZnO nanoparticles doped with 0.5 mol% Nb exhibited an optimum NO_2 response of ~1640 and a very fast response time (27 s) for NO_2 concentration of 4 ppm at 300^oC. The low NO_2 detection limit of 0.5 mol% Nb-doped was estimated to be 20 ppb at 300^oC. Furthermore the 0.5 mol% Nb-doped sensor films are highly sensitive to low NO_2 concentrations (4 ppm) at 350^oC. The sensing films showed lower gas response to other gases: CO (1000 ppm), C_2H_5OH (1000 ppm) and acetone (1000 ppm) suggesting the use of 0.5 mol% Nb-doped sensing films for selective detection of these four gases.

REFERENCES

1. Sberveglieri G., *Gas Sensors-Principles, Operation and Developments*, Kluwer Academic, Dordrecht, 1992.

2. Chou J., *Hazardous Gas Monitors-A Practical Guide to Selection, Operation and Applications*, SciTech, North Carolina, 2000.

3. Yamazoe N., Kurokawa Y., Seiyama T., Effects of additive on semiconductor gas sensor, *Sens. Actuators* B: Chem., 1983, **4,** 283−289.

4. Qin L., Xu J., Dong X., Pan Q., Cheng Z., Xiang Q., Li F., The template-free synthesis of square-shaped SnO_2 nanowires: the temperature effect and acetone gas sensors, *Nanotechnology*, 2008, **19**, 185705.1−185705.8.

5. Liao L., Lu H.B., Shuai M., Li J.C., Liu Y.L., Liu C., Shen Z.X., Yu T., A novel gas sensor based on field ionization from ZnO nanowires: moderate working voltage and high stability, *Nanotechnology*, 2008, **19**, 175501.1−175501.5.

6. Rout C.S., Hegde M., Rao C.N.R., H_2S sensors based on tungsten oxide nanostructures, *Sens. Actuators B: Chem.,* 2008, **128**, 488−493.

7. Kaur M., Jain N., Sharma K., Bhattacharya S., Roy M., Tyagi A.K., Gupta S.K., Yakhmi J.V., Room-temperature H_2S gas sensing at ppb level by single crystal In_2O_3 whiskers, *Sens. Actuators B: Chem.*, 2008, **133**, 456−461.

8. Raible I., Burghard M., Schlecht U., Yasuda A., Vossmeyer T., V_2O_5 nanofibres: novel gas sensors with extremely high sensitivity and selectivity to amines, *Sens. Actuators B: Chem.*, 2005, **106**, 730−735.

9. Li Z., Zhang H., Zheng W., Wang W., Huang H., Wang C., MacDiamid A.G., Wei Y., Highly sensitive and stable humidity nanosensors based on LiCl doped TiO_2 electrospun nanofibers, *J. Am. Chem. Soc.,* 2008, **130,** 5036−5037.

10. Sadek A.Z., Choopun S., Wlodarski W., Ippolito S.J., Kalantar-zadeh K., Characterization of ZnO nanobelt-based gas sensor for H_2, NO_2, and hydrocarbon sensing, *IEEE Sens. J.*, 2007, **7**, 919−924.

11. Zhang F.X., *Sensors Application and its Circuit Selection*, Electronics Industry, Beijing, 1993.

12. Saxena V., Aswal D.K., Kaur M., Koiry S.P., Gupta S.K., Yakhmi J.V., Kshirsagar R.J., Deshpande S.K., Enhanced NO_2 selectivity of hybrid poly(3-hexylthiophene):ZnO-nanowire thin films, *Appl. Phys. Lett*., 2007, **90**, 043516.1−043516.3.

13. Shimizu Y., Egashira M., Basic aspects and challenges of semiconductor gas sensors, *MRS Bull*. 1999, **24**, 18−24

14. Guidotti T.L., The higher oxides of nitrogen: inhalation toxicology, *Environ. Res.* 1978, **15**, 443−472.

15. Richters A., Kuraitis K., Inhalation of NO_2 and blood borne cancer cell spread to the lungs, *Arch. Environ. Occup. H.,* 1981, **36**, 36−39.

16. Baratto C., Sberveglieri G., Onischuk A., Caruso B., Stasio S.D., Low temperature selective NO_2 sensors by nanostructured fibres of ZnO, *Sens. Actuators B: Chem*., 2004, **100**, 261−265.

17. Talazac L., Brunet J., Battut V., Blanc J.P., Pauly A., Germain J.P, Pellier S., Soulier C., Air quality evaluation by monolithic InP-based resistive sensors, *Sens. Actuators B: Chem.*, 2001, **76**, 258–264.

18. Yamazoe N., G Sakai., Shimanoe K., Oxide Semiconductor Gas Sensors, *Catal. Surv. Asia*, 2003, **7**, 63–75,

19. Seiyama T., Kato A., Fujiishi K., Nagatani M., A new detector for gaseous components using semiconductive thin films, *Anal. Chem.,* 1962, **34**, 1502–1503.

20. Taguchi N., Jap. Patent, 45–38200, 1962.

21. Bai S.L., Chen L.Y., Yang P.C., Chen A.F., Liu C.C., Sn/In/Ti nanocomposite sensor for CH$_4$ detection, *Sens. Actuators B: Chem.*, 2008, **135**, 1–6.

22. Juna J.H., Yuna J., Choa K., Hwangb I.S, Leeb J.H, Kima S, Necked ZnO nanoparticle-based NO$_2$ sensors with high and fast response, *Sens. Actuators B: Chem.*, 2009, **140**, 412–417.

23. Eggins, B. R. *Chemical Sensors and Biosensors. West Sussex* : John Wiley & Sons, New York., 2002.

24. Ramgir N.S., Mulla I.S., Vijayamohanan K.P., A room temperature nitric oxide sensor actualized from Ru-doped SnO$_2$ nanowires, *Sens. Actuators B: Chem.*, 2005, **107**, 708–715.

25. Qian L.H., Wang K., Li Y., Fang H.T., Lu Q.H., Ma X.L., Au nanoparticles enhance CO oxidation onto SnO$_2$ nanobelt, *Mater. Chem. Phys.,* 2006, **100**, 82–84.

26. Morrison S.R., Semiconductor Gas Sensors, *Sens. Actuators B: Chem.*, 1982, **2,** 329–341.

27. Oha E., Choib H.Y., Jungc S.H., Choc S., Kima J.C., Leec K.H., Kangd S.W., Kimd J., Yund J.Y, Jeonga S.H., High-performance NO_2 gas sensor based on ZnO nanorod grown by ultrasonic irradiation, *Sens. Actuators B: Chem.*, 2009, **141**, 239−243.

28. Shoulia B., Liangyuanb C., Dianqinga L., Wenshenga Y., Pengchenga Y., Zhiyonga L., Aifana C., Liub C.C., Different morphologies of ZnO nanorods and their sensing property, *Sens. Actuators B: Chem.*, 2010, **146**, 129−137.

29. Calestania D., Zhaa M., Moscaa R., Zappettinia A., Carottab M.C., Nataleb V.D., Zanottia L., Growth of ZnO tetrapods for nanostructure-based gas sensors, *Sens. Actuators B: Chem.*, 2010, **144**, 472−478

30. Ferroa R., Rodríguez J.A., Bertrand P., Henry M., Poleunis C., Response enhancement of sprayed ZnO thin film-based NO_2 sensor by indium-doping, *Rev. Mex. Fis.,* 2006, **52,** 23−25.

31. Tamaekong N., Liewhiran C., Wisitsoraat A., Phanichphant S., Ultra-rapid CO gas detection by a gas sensor based on flame-spray-made Pt/ZnO nanoparticles, *Key Eng. Mater., Vols. 2010, **421-422,*** 332−33.

32. Chang S.J., Hsueh T.J., Chen I.C., Huang B.R., Highly sensitive ZnO nanowire CO sensors with the adsorption of Au nanoparticles, *Nanotechnology,* 2008, **19**, 175502−175506.

33. Shishiyanu S.T., T.S. Shishiyanu, O.I. Lupan, Sensing characteristics of tin-doped ZnO thin films as NO_2 gas sensor, *Sens. Actuators B: Chem.*, 2005, **107**, 379−386.

190

34. Tamaekong N., Liewhiran C., Wisitsoraat A., Phanichphant S., Flame-spray-made undoped zinc oxide films for gas sensing applications, *Sensors-Basel.*, 2010, **10**, 7863–7873.

35. Sahay P.P, Tewari S., Jha S., Shamsuddin M., Sprayed ZnO thin films for ethanol sensor. *J. Mater. Sci.,* 2005, **40**, 4791–4793.

36. Liewhiran C., Phanichphant S., Effects of palladium loading on the response of a thick film flame-made ZnO gas sensor for detection of ethanol vapor. *Sensors-Basel.,* 2007, **7,** 1159–1184.

37. Hongsith N., Viriyaworasakul C., Mangkorntong P., Mangkorntong N., Choopun S., Ethanol sensor based on ZnO and Au-doped ZnO nanowires, *Ceram. Int.,* 2008, **34**, 823–826.

38. Shishiyanu S.T., Shishiyanu T.S., Lupan O.I., Sensing characteristics of tin-doped ZnO thin films as NO_2 gas sensor, *Sens. Actuators B: Chem.*, 2005, **107,** 379–386.

39. Sawada H., Wang R., Sleight A.W., An electron density residual study of zinc oxide, *J. Solid State Chem.,* 1996, **122**, 148–150.

40. Sawada H., Residual electron density study of α-aluminum oxide through refinement of experimental atomic scattering factors, *Mater. Res. Bull.* 1994, **29**, 127–133.

41. Wong-Ng W., McMurdie H.F., Hubbardl C.R., Mighell A.D., JCPDS-ICDD Research Associateship (Cooperative Program with NBS/NIST), *J. Res. Natl. Inst. Stan.*, 2001, **106**, 1013–1028.

42. Manno D., Micocci G., Rella R., Serra A., Taurino A., Tepore A., Titanium oxide thin films for NH_3 monitoring: structural and physical characterizations, *J. Appl. Phys.*, 1997, **82**, 54–59.

43. Stambolova I., Konstantinov K., Khristova M., Peshev P., NO sensitivity of spinel type Zn_2SnO_4 spray deposited films, *Phys. Status Solidi A,* 1998, **167**, R11–R12.

44. Yamada Y., Seno Y., Masuoka Y., Yamashita K., Nitrogen oxides sensing characteristics of Zn_2SnO_4 thin film, Sens. *Actuators B: Chem.*, 1998, **49**, 248–252.